Polarized NORTIA accumulation in response to pollen tube arrival at synergids promotes fertilization.

Yan Ju[1,2,6], Jing Yuan[1,2,6], Daniel S. Jones[4,5], Weiwei Zhang[2,3], Christopher J. Staiger[1,2,3], and Sharon A. Kessler[1,2,7,*]

[1]Department of Botany and Plant Pathology, Purdue University, West Lafayette, Indiana 47907, USA
[2]Purdue Center for Plant Biology, Purdue University, West Lafayette, Indiana 47907, USA
[3]Department of Biological Sciences, Purdue University, West Lafayette, Indiana 47907, USA
[4]Department of Biological Sciences, Auburn University, Auburn, Alabama 36849, USA (current address)
[5]Department of Microbiology and Plant Biology, University of Oklahoma, Norman, Oklahoma 73019, USA
[6]These authors contributed equally
[7]Lead Contact
* Correspondence: sakessler@purdue.edu

Summary

Signal-mediated regulation of protein trafficking is an elegant mechanism to control the delivery of molecules to a precise location for critical signaling events that occur over short time frames. During plant reproduction, the FERONIA receptor complex is critical for intercellular communication that leads to gamete delivery, however the impact of the FERONIA signal transduction cascade on protein trafficking in synergid cells remained unknown. Live-imaging of pollen tube reception revealed that a key outcome of FERONIA signaling is polar accumulation of the MLO protein NORTIA at the filiform apparatus in response to signals from an arriving pollen tube. Artificial delivery of NORTIA to the filiform apparatus is sufficient to bypass the FERONIA signaling pathway and to promote interspecific pollen tube reception. We propose that polar accumulation of NORTIA leads to the production of a secondary booster signal to ensure that pollen tubes burst to deliver the sperm cells for double fertilization.

Introduction

Intercellular communication is central to the proper development and maintenance of all multicellular organisms. During this communication, signals from one cell are perceived by receptors in another cell and translated into various subcellular responses. These responses include signal transduction cascades leading to transcription of other genes, calcium signaling, and trafficking of proteins to different organelles or regions of the cell. A well-studied example of signal-induced protein trafficking in plant development is the redistribution of the PIN polar auxin transporters to different sides of the cell during important developmental events such as embryo patterning, leaf initiation and lateral root initiation (Naramoto, 2017; Petrasek et al., 2006; Salanenka et al., 2018). Membrane proteins also change their polarity in response to signaling induced by pathogen attack. In response to powdery mildew infection, the tSNARE protein PENETRATION RESISTANCE 3 (PEN3) is recruited to the fungal penetration site in a lipid Flippase ALA3-dependent mechanism (Underwood et al., 2017; Underwood and Somerville, 2013). Similarly, members of the MILDEW RESISTANCE LOCUS-O (MLO) family of seven-transmembrane proteins redistribute in the plasma membrane in order to accumulate at attempted fungal penetration sites (Bhat et al., 2005; Qin et al., 2020). Changes in the polarity of these membrane proteins are tightly regulated and critical for cell-to-cell communication. In plants, most intercellular communication occurs between cells that are genetically identical and connected by adjoining cell walls. One exception is pollination, in which pollen (the male gametophyte) is released from an anther, transported to a receptive stigma, and produces a tip-growing pollen tube (PT) that grows through the female tissues of the pistil and delivers the two sperm cells to the female gametophyte (also known as the embryo sac, Figure 1A). The PT's journey through the pistil requires cell-to-cell interactions with the female that allows water and nutrient uptake and enables the detection of important guidance cues toward the female gametes (Johnson et al., 2019).

In the model plant *Arabidopsis thaliana (A. thaliana)*, complex signaling events ranging from pollen landing on the stigma to fusion of gametes occur over several hours. Most of our knowledge about the signaling pathways involved along the PT's journey through the female is limited to the final stages of pollination and involve a highly specialized pair of female gametophyte cells known as synergids. During female gametophyte development, meiosis followed by three rounds of mitosis produce the egg cell and central cell along with two synergid cells flanking the egg cell and three antipodal cells on the chalazal end of the embryo sac (Drews and Yadegari, 2002) (Figure 1A). The synergids are accessory cells that control the

behavior of the PT during the final stages of pollination. Before PT arrival, they secrete cysteine-rich LURE peptides that act as short-range PT attractants that are recognized by receptor-like kinases (RLKs) in the tip of the PT to regulate the direction of PT growth and guide the PT to the micropyle of the ovule (Okuda et al., 2009; Takeuchi and Higashiyama, 2016; Wang et al., 2016). After PT arrival, the synergids communicate with the PT to induce changes that result in PT rupture and delivery of the sperm cells in a process known as PT reception (Johnson et al., 2019; Kessler and Grossniklaus, 2011). Mutations in genes that regulate communication between the synergids and PT result in a PT overgrowth phenotype in which the PTs are attracted normally to the ovules, but do not get the signal to burst and release the sperm cells. Presumably, synergid-induced changes in the cell wall of the PT tip do not occur in these mutants, therefore the PT continues to grow and coil inside the embryo sac. Synergid-expressed genes that participate in PT reception include the FERONIA (FER) receptor-like kinase, the GPI-anchored protein LORELEI (LRE), and the MLO protein NORTIA (NTA, also known as AtMLO7) (Capron et al., 2008; Escobar-Restrepo et al., 2007; Kessler et al., 2010; Li et al., 2015; Liu et al., 2016).

The subcellular localization of important PT reception proteins is not always predictive of their function in communicating with the PT. As expected for early response proteins, both FER and LRE are expressed in synergids where they localize in or near a specialized region called the filiform apparatus, a membrane-rich area located at the micropyle end of the synergids (Capron et al., 2008; Escobar-Restrepo et al., 2007; Huck et al., 2003; Li et al., 2015; Lindner et al., 2015; Liu et al., 2016; Rotman et al., 2003). The filiform apparatus is thought to be important for the secretion of attractant peptides and is the first site of interaction between the PT and synergid prior to PT reception (Huang and Russell, 1992; Leshem et al., 2013; Mansfield et al., 1991). In contrast, before PT arrival, NTA is localized to a Golgi-associated compartment within the synergid and absent from the filiform apparatus (Jones et al., 2017). At the end of PT reception, NTA protein is only detected at the filiform apparatus, indicating that this protein changes its subcellular localization during PT reception (Kessler et al., 2010). This suggests that PT-triggered regulation of the synergid secretory system may be a crucial subcellular response to PT arrival and that NTA function may be related to its subcellular distribution; however, the precise timing and significance of NTA's redistribution remain unclear.

Here, we use a live-imaging system to determine the timing and significance of the polar accumulation of NTA at the filiform apparatus and to further characterize synergid subcellular

dynamics during PT reception in response to PT arrival at the entrance to the female gametophyte. While major subcellular compartments remain evenly distributed throughout the synergids during PT reception, NTA actively accumulates at the filiform apparatus. Manipulation of NTA's subcellular localization with domain swaps and a Golgi retention signal revealed that filiform apparatus localization of NTA (faNTA) is necessary and sufficient for MLO function in PT reception and can bypass the FER/LRE signal transduction cascade. faNTA also enhances the ability of *A. thaliana* synergids to receive interspecific PTs from *Arabidopsis lyrata* (*A. lyrata*) in a FER-dependent manner. We propose that faNTA functions to provide a secondary "booster signal" in the micropyle to ensure that the attracted PT bursts for the completion of double fertilization, thereby defining a new level of redundancy in the PT-synergid signaling mechanism.

Results

NTA dynamically accumulates at the filiform apparatus during PT reception

PT reception requires synergids to recognize the approaching PT and to send signals back to the PT that result in release of the sperm cells at the correct time and place so that double fertilization can be completed. Based on static images, we previously reported that NTA-GFP fusion protein localizes to a Golgi-associated compartment in synergids prior to PT attraction (Jones et al., 2017). When imaged after PT reception, NTA-GFP is concentrated at the micropylar end of the synergid (in or near the filiform apparatus) (Kessler et al., 2010). NTA-GFP does not accumulate at the filiform apparatus in *fer* ovules with PT overgrowth, suggesting that FER-mediated signaling during PT reception triggers NTA-GFP redistribution that in turn contributes to the interaction of the synergid with the PT (Kessler et al., 2010)(Figure S1A-C). An alternative hypothesis is that PT rupture triggers NTA-GFP redistribution and is a symptom of PT reception rather than an important contributor to the signaling pathway. To distinguish between these two possibilities, we used a semi-*in vivo* pollination system combined with time-lapse spinning disk confocal microscopy to determine the timing of NTA-GFP redistribution during the PT reception process. In the semi-*in vivo* system, PTs grow out of a cut style and are attracted to ovules arranged on pollen germination media (Palanivelu and Preuss, 2006). This system has previously been used to quantify and track PT attraction to ovules and to image $[Ca^{2+}]_{cyto}$ reporters during PT reception (Denninger et al., 2014; Hamamura et al., 2012; Hamamura et al., 2014; Hamamura et al., 2011; Huang et al., 2015; Ngo et al., 2014). To follow subcellular changes in NTA-GFP protein localization before, during, and after PT arrival, we used pollen from plants expressing the pollen-specific *AUTOINHIBITED* Ca^{2+}-

ATPase9$_{pro}$*::DsRed* (*ACA9*$_{pro}$*::DsRed*) reporter and ovules expressing *NTA*$_{pro}$*::NTA-GFP* in the semi-*in vivo* system. Approximately 4 h after pollination, PTs emerged from the style onto the media and were attracted to ovules (Figure 1B). Fluorescence images in both channels were collected every 5 min from when a PT approached an ovule until after the PT ruptured inside the ovule. In ~83% (n = 93) of the ovules that attracted a PT that successfully burst to deliver the sperm cells, NTA-GFP accumulated at the filiform apparatus of the synergids (Figures 1C-1E). The rest of the ovules (~17%) attracted PTs that stopped growing in the micropyle and did not rupture. In these ovules, NTA-GFP did not accumulate at the filiform apparatus. To exclude the possibility that prolonged imaging causes stress in synergids which leads to filiform apparatus accumulation of NTA-GFP, we analyzed neighboring ovules that did not attract PTs but were imaged together with ovules that attracted PTs. NTA-GFP did not accumulate at the filiform apparatus in these ovules (Figure 1F). Likewise, ovules that were incubated on pollen germination media without a pollinated pistil (Figures 1F, S1G and S1H) and imaged over the same time frame did not accumulate NTA-GFP at the filiform apparatus. These data indicate that PT arrival is necessary for NTA-GFP accumulation at the filiform apparatus rather than being retained in the Golgi, and that this accumulation is not an artifact of the semi-*in vivo* imaging system (Figure 1F).

Our semi-*in vivo* system also allowed us to determine the timing of NTA-GFP accumulation at the filiform apparatus in relation to the position of the PT as it approached the synergids. We defined the 0 min timepoint as the time where the PT just reached the micropylar opening of the ovule (Figure 1C, Movie S1). In all cases, the shift of NTA-GFP signal from the Golgi to the filiform apparatus also started from this time point. During the following 30–50 min, PTs grew through the micropyle region of ovule and arrived at the filiform apparatus of the receptive synergid. During this timeframe, half to three quarters of the NTA-GFP signal moved to the micropylar end of synergids, indicating that the approach of the PT triggers NTA-GFP accumulation at the filiform apparatus. As reported in (Ngo et al., 2014) and (Denninger et al., 2014), the arriving PTs paused their growth outside the filiform apparatus for 30–50 min, presumably for cell-to-cell communication. During this period, the NTA-GFP signal continued to shift toward the filiform apparatus. At 70–80 min after PT arrival at the micropyle, NTA-GFP signal was only detected at the filiform apparatus and PTs resumed growth and later ruptured to release the sperm cells (Figures 1C and 1D, Movies S1). Even though only one of the synergids receives the PT, NTA-GFP accumulated at the filiform apparatus in both synergids in response

to PT arrival, similar to the activation of $[Ca^{2+}]_{cyto}$ oscillations in both synergids during PT reception reported in (Ngo et al., 2014).

Golgi do not concentrate at the filiform apparatus during PT reception

We previously determined that NTA is sequestered in a Golgi-associated compartment in synergids that have not attracted a PT (Jones et al., 2017). Our live-imaging data suggest that NTA-GFP is selectively moved out of the Golgi and transported to the filiform apparatus in response to PT arrival. However, it is possible that the observed NTA-GFP accumulation at the filiform apparatus is a result of massive reorganization of subcellular compartments. To distinguish between these possibilities, we first investigated the behavior of the Golgi in synergids during PT reception. We used the semi-*in vivo* imaging system described above with a synergid-expressed Golgi marker (*LRE_{pro}::*Man49-mCherry) co-expressed with NTA-GFP (Jones et al., 2018). In all replicates, the Golgi marker was distributed throughout the synergids, excluded from the filiform apparatus, and co-localized with NTA-GFP as reported previously (Figure 2A, n = 93). When a PT approached the synergids, NTA-GFP accumulated at the filiform apparatus of the synergids as observed previously (Figure 1), but the Golgi-mCherry marker remained consistently distributed throughout the synergids and did not concentrate near the filiform apparatus (Figure 2B). In order to examine the behavior of the Golgi during later stages of PT reception, we used *LRE_{pro}::Man49-mCherry* and pollen that expresses GFP (*$Lat52_{pro}$::GFP*). In all cases, the Golgi marker remained randomly distributed throughout the synergids, even after PT rupture (Figures 2C and 2D, Movies S2, n = 106). These results indicate that the accumulation of NTA-GFP at the filiform apparatus during PT reception is not linked to mass redistribution of Golgi. Likewise, fluorescent markers for the trans-Golgi network (TGN), endoplasmic reticulum (ER), and peroxisomes did not change their distributions to accumulate at the filiform apparatus during PT arrival (Figure S2 and Movies S3-S5), confirming that NTA accumulation at the filiform apparatus is not just an artifact of major subcellular reorganization.

PT-independent targeting of NTA to the filiform apparatus is not toxic to the synergids

The selective targeting of NTA-GFP from the Golgi to the filiform apparatus during PT arrival (Figures 1 and 2) suggests that NTA trafficking to the PT/synergid interface is important for the intercellular communication process that occurs between the PT and synergids. In *nta-1* mutants, around 30% of ovules display PT overgrowth and fail to complete double fertilization, but the other 70% are fertilized normally (Kessler et al., 2010). This indicates that NTA is not

absolutely required for PT reception, but may function as a modifier of the signaling pathway. Since FER signaling in the synergids leads to cell death as PT reception is completed (Escobar-Restrepo et al., 2007; Huck et al., 2003; Rotman et al., 2003), NTA trafficking to the filiform apparatus could be a mechanism to regulate this death and would thus require sequestration of "toxic" NTA in the Golgi before PT arrival. To test this hypothesis, we took advantage of sequence variation leading to differential subcellular localization of MLO proteins to manipulate the subcellular localization of NTA. When expressed in synergids, other proteins from the Arabidopsis MLO family have different subcellular localization patterns, indicating that specific sequences within the MLOs direct them to different parts of the secretory system (Jones and Kessler, 2017). MLO1-GFP localizes at the filiform apparatus when it is ectopically expressed under control of the synergid-specific *MYB98* promoter and cannot complement the *nta-1* PT reception phenotype (Figures 3B and 3G)(Jones et al., 2017). Domain swaps between different regions of NTA and MLO1 revealed that the C-terminal cytoplasmic tail of MLO1 (NTA-MLO1^{CTerm}, see diagram in Figure 3C) was sufficient to direct the fusion protein to the filiform apparatus of the synergids, in a pattern very similar to MLO1-GFP (Figure 3B), therefore NTA-MLO1^{CTerm} was named faNTA. Quantification of the GFP signal along the length of the synergids from the chalazal end to the filiform apparatus in NTA-GFP, MLO1-GFP, and faNTA-GFP synergids confirmed that the MLO1 tail was sufficient to cause NTA protein accumulation at the filiform apparatus (Figures 3A-3C). In MLO1-GFP and faNTA-GFP ovules, the majority of GFP signal was detected within the 20-40% of synergid length near the micropylar pole and most of the signal overlapped with the diffuse FM4-64 staining at the filiform apparatus (Figure 3F). In contrast, wild-type NTA-GFP is excluded from the filiform apparatus in unpollinated synergids (Figure 3A and (Jones et al., 2017).

The successful manipulation of NTA subcellular localization provided a tool for determining the functional relevance of NTA redistribution. We introduced faNTA-GFP into *nta-1* plants and used the percentage of unfertilized ovules as a measure for the ability of the fusion construct to complement the *nta-1* phenotype of unfertilized ovules caused by PT overgrowth (Kessler et al., 2010). Synergid-expression of *faNTA-GFP* rescued the *nta-1* PT reception phenotype (Figure 3G), indicating that 1) the MLO1^{CTerm} domain is functionally equivalent to the NTA^{CTerm} domain when the protein is localized at the filiform apparatus and 2) premature targeting of NTA to the filiform apparatus is not toxic to synergids.

Polar accumulation of NTA at the filiform apparatus is necessary for PT reception

Early targeting of faNTA-GFP to the filiform apparatus was sufficient to complement the *nta-1* PT reception phenotype, but did not give an indication of whether filiform apparatus targeting is necessary for NTA function. Since NTA accumulation is triggered by the arrival of a growing PT, drugs that block membrane protein trafficking are not appropriate to inhibit NTA accumulation at the filiform apparatus because they would also inhibit PT growth. Therefore, we attempted to inhibit NTA trafficking to the filiform apparatus by adding a Golgi retention signal (RNIKCD) to the C-terminus of our MLO-GFP variants. RNIKCD causes Golgi-retention when added to proteins that would normally be targeted to the trans-Golgi network and tonoplast (Gao et al., 2012). In order to test if RNIKCD also retains MLO proteins in the Golgi, we added it to the C-terminus of MLO1 (MLO1-GFP-RNIKCD) and NTA (NTA-GFP-RNIKCD) and co-infiltrated tobacco leaves with these constructs and the Golgi-mCherry marker (*35S::Man49-mCherry*). Both NTA-GFP and NTA-GFP-RNIKCD co-localize with Golgi-mCherry marker in tobacco epidermis (Figure S3A), as was previously reported for NTA-GFP (Jones et al., 2017). However, in contrast to MLO1-GFP which accumulates at the plasma membrane, most of the MLO1-GFP-RNIKCD was retained in the Golgi (Figure S3A). In order to assess whether RNIKCD changes NTA localization to a different subcellular compartment, we co-infiltrated tobacco leaves with 35S::NTA-Cer3 (Jones et al., 2017) and pFER::NTA-GFP-RNIKCD. These two proteins colocalized (Figure S3B), indicating that the RNIKCD does not alter the Golgi localization of NTA in cells that have not received a "relocalization" signal from a PT. We next added RNIKCD to $MYB98_{pro}$-driven NTA-GFP and faNTA-GFP (NTA-GFP-RNIKCD and faNTA-GFP-RNIKCD) and transformed the constructs into *nta-1* and Golgi-mCherry plants for functional and subcellular localization studies, respectively. In synergids of emasculated ovules, both NTA-GFP-RNIKCD and faNTA-GFP-RNIKCD fusion proteins were retained in the cytoplasmic area of the synergids and partially co-localized with the Golgi marker (Figure S3C). Synergid-expressed NTA-GFP-RNIKCD and faNTA-GFP-RNIKCD could partially rescue the *nta-1* PT reception phenotype (Figure 3G). The partial rescue could be due to insufficient transgene expression or leakiness in the Golgi retention signal. The lines shown in Figure 3G express similar (*faNTA-GFP*, *NTA-GFP-RNIKCD* #1 and *faNTA-GFP-RNIKCD* #2) or higher (*MLO1-GFP*, *NTA-GFP-RNIKCD* #2 and *faNTA-GFP-RNIKCD* #1) levels of MLO-GFP compared to NTA-GFP (Figure S3D), suggesting that the inability of MLOs to rescue *nta-1* is not caused by inadequate transgene expression. However, the NTA-GFP-RNIKCD fusion protein could sometimes be detected at the filiform apparatus in ovules that had attracted PTs, but at a much lower rate than NTA-GFP (Figures S3E and S3F), indicating that the Golgi retention signal impairs the ability of NTA to accumulate at the filiform apparatus, but does not absolutely

prevent it. Nonetheless, our data indicate that faNTA is both necessary and sufficient for PT reception.

faNTA bypasses FER signaling and promotes PT reception by reducing PT overgrowth

Our live imaging experiments revealed that NTA selectively moves out of Golgi and concentrates at the filiform apparatus of the synergids in response to signals from an arriving PT. In *fer-1* ovules, NTA-GFP does not accumulate at the filiform apparatus during PT reception (Figures S1A-C)(Kessler et al., 2010), placing NTA downstream of FER. Since FER function is required for NTA accumulation at the filiform apparatus, one hypothesis is that the FER-triggered signal transduction cascade controls polar trafficking of NTA, and after arriving at the filiform apparatus, NTA could require additional FER function to communicate with the PT. An alternative hypothesis is that FER is only responsible for NTA's redistribution to the filiform apparatus, but does not participate in later stages of the PT-synergid interaction that leads to PT rupture. To distinguish between these possibilities, we took advantage of faNTA because it is localized to the filiform apparatus before PT arrival and is able to rescue the *nta-1* infertility phenotype. Synergid-expressed *faNTA-GFP* was introduced into *fer-1* and plants that were homozygous for *faNTA-GFP* and either heterozygous or homozygous for *fer-1* (*faNTA;fer-1/+ or faNTA;fer-1*) were obtained. In *fer-1* synergids, faNTA-GFP accumulated at the filiform apparatus (Figure 4B), while wild-type NTA was excluded from the filiform apparatus (Figure 4C). *fer-1* has an average of 80.8% unfertilized ovules due to PT overgrowth, but when faNTA-GFP was introduced to *fer-1*, the unfertilized ovule rate of *faNTA;fer-1* was reduced to 41.5%, indicating partial suppression of *fer-1* infertility (Figures 4D-4F). Aniline blue staining of pollinated pistils revealed that the increase in fertility in *faNTA;fer-1* is due to a decrease in PT overgrowth (Figure 4G). In pollinated *faNTA;fer-1* pistils, some ovules had normal PT reception and were fertilized (Figure 4H arrow) while other ovules displayed PT overgrowth and did not get fertilized (Figure 4H arrowhead).

In order to test whether the suppression of the *fer-1* phenotype was due to increased NTA dosage in the transgenic plants, we also tested whether wild-type NTA expressed under control of the MYB98 promoter could suppress *fer-1* infertility. The fertility of *NTA;fer-1/+* is comparable to the fertility of *fer-1/+*, and both have significantly more unfertilized ovules than that of *faNTA;fer-1/+* (Figures 4F, S4E and S4F), confirming that FER is required for NTA accumulation at the filiform apparatus and that overexpressing wild-type NTA in the synergid does not bypass the FER signal transduction cascade. The *fer-1* allele is tightly linked to a kanamycin resistance

gene (Kan^R), which could be used for genetic analysis. In the F2 progeny from a self-pollinated *fer-1/+* plant, the percent of Kan^R seedlings is 54.8% due to female gametophytic lethality associated with the *fer-1* mutation. When *faNTA-GFP* is expressed in *fer-1/+*, Kan^R plants in the F2 progeny increased to 63.8%, indicating increased transmission of the *fer-1* allele. Furthermore, the percentage of homozygous *fer-1* plants increased from 7.9% to 14.5% (Table S1), confirming that filiform apparatus accumulation of NTA is sufficient to bypass the FER signal transduction cascade by promoting PT bursting and delivery of the sperm cells. However, when *NTA-GFP* is expressed in *fer-1/+*, the percentage of Kan^R plants was 56.7%, which is comparable to *fer-1/+* (54.8%), and the percentage of homozygous *fer-1* plants was 6.3% (Table S1), confirming that wild-type NTA does not bypass FER signaling.

faNTA also bypasses LRE signaling and promotes PT reception

We predicted that faNTA would also suppress PT overgrowth in other mutants that have been linked to the FER signaling pathway. LRE is a GPI-anchored protein that is localized to the filiform apparatus in the synergid and interacts with FER as a co-receptor to control PT reception (Li et al., 2015). NTA-GFP does not accumulate at the filiform apparatus in response to signals from the arriving PT in *lre-7* ovules (Figures S1D-F), suggesting that NTA is also downstream of LRE. To test whether faNTA could also bypass LRE function, synergid-expressed *faNTA-GFP* was introduced into *lre-7* mutant and plants that were homozygous for both *faNTA-GFP* and *lre-7* (*faNTA;lre-7*) were obtained. In unfertilized ovules, the *lre-7* mutation does not affect faNTA-GFP accumulation at the filiform apparatus (Figure 5A). As expected for a co-receptor with FER, faNTA-GFP also suppressed *lre-7* infertility, with 29.6% unfertilized ovules in *faNTA;lre-7* pistils compared to 69.0% unfertilized ovules in *lre-7* pistils due to PT overgrowth (Figures 5C, 5D, and 5G). The T-DNA insertion in *lre-7* contains a Basta resistance gene (Liu et al., 2016), so we used the same approach as with *fer-1* to test the segregation of progeny from self-pollinated plants. 57.3% of F2 progeny from *lre-7/+* are Basta-resistant ($Basta^R$), while the F2 progeny from *faNTA;lre-7* plants are 61.4% $Basta^R$ (Table S1), confirming the suppression effect of faNTA on *lre-7*. The $Basta^R$:$Basta^S$ ratio from *lre-7/+* (1.34) is consistent with that in a previous transmission efficiency study (Liu et al., 2016).

As expected, faNTA could suppress PT overgrowth in *fer* and *lre*, two mutants that have been genetically and biochemically connected. In order to determine whether faNTA suppression is specific to the FER pathway, we also tested the ability of faNTA to suppress other PT overgrowth mutants that are independent from FER and LRE. Neither *turan* (*tun*), a mutant in a

uridine diphosphate (UDP)-glycosyltransferase superfamily protein that is thought to mediate PT reception through regulation of protein glycosylation in the synergids (Lindner et al., 2015) nor the *myb97 myb101 myb 120* triple mutant which causes PT overgrowth from the male side (Leydon et al., 2013) were suppressed by faNTA (Figure 5B, 5E-5H and Table S1). Thus, faNTA is not a general promoter of PT rupture and is instead specific to the FER/LRE pathway.

faNTA promotes interspecific PT reception

When *A. lyrata* pollen grains are used to pollinate *A. thaliana* stigmas, *A. lyrata* PTs are guided to *A. thaliana* embryo sacs, but often coil and fail to burst in a manner resembling the *nta-1*, *lre-7*, and *fer-1* mutant PT overgrowth phenotypes (Muller et al., 2016). This phenotype is dependent on the genetic background of *A. thaliana*, with natural variation leading to PT overgrowth rates ranging from 10.2% to 90.9% in *A. thaliana* accessions pollinated with *A. lyrata* pollen (Muller et al., 2016) and suggests miscommunication between *A. lyrata* PTs and *A. thaliana* synergids during PT reception. To test whether faNTA is sufficient to overcome the interspecific PT reception defect, we crossed *A. lyrata* pollen onto a series of *A. thaliana* genotypes and observed PT overgrowth with aniline blue staining 2 days after pollination. In the control cross of *A. thaliana*$_{Ws\text{-}2}$ X *A. lyrata,* 56.5% of ovules had PT overgrowth (Figure 6A), which is consistent with a previous report (Muller et al., 2016). In *nta-1* x *A. lyrata*, the PT overgrowth rate increased to 80.7%, indicating a decreased ability for *nta-1* synergids to communicate with foreign PTs. faNTA-GFP was able to partially suppress interspecific PT overgrowth rates to 25.4%. Wild-type NTA-GFP could also reduce interspecific PT overgrowth to 29.6%, but adding the Golgi retention to signal RNIKCD to this construct inhibited this suppression (Figure 6A), revealing that NTA accumulation at the filiform apparatus promotes reception of *A. lyrata* PTs. For these experiments, we used the synergid-specific MYB98 promoter, which leads to higher expression than the native NTA promoter. Our interspecific cross data suggests that not only faNTA but also high levels of wild-type NTA are sufficient to enhance PT reception, presumably due to an increase in the pool of protein that is ready to accumulate at the filiform apparatus in response to signals from the arriving PT. A similar result was seen when Lp2-2, an *A. thaliana* accession with high levels of interspecific PT overgrowth, was transformed with NTA-GFP and faNTA-GFP. Both constructs were able to suppress *A. lyrata* PT overgrowth, with faNTA having a stronger effect (Figure 6C). To exclude the possibility that the faNTA suppression effect is caused by the MLO1 C-terminus, we crossed *MLO1-GFP;nta-1* with *A. lyrata* and found that there is no significant change compared to *nta-1* (Figure 6A). We also tested whether FER is required for the faNTA suppression of interspecific PT

overgrowth. *fer-1* pistils pollinated with *A. lyrata* have PT overgrowth in almost 100% of ovules (Figure 6B). This phenotype was not suppressed by faNTA (Figure 6B), indicating that both proteins are required for *A. lyrata* PT rupture.

Discussion

Successful pollination and production of seeds requires a series of signaling events between the male gametophyte (PT) and both sporophytic and gametophytic cells of the female. In this study, we used live imaging and artificial manipulation of protein targeting to define the role of signal-induced polar localization of a membrane protein, NTA, in PT reception, the critical communication pathway between the synergid and PT that leads to the delivery of male gametes to the female gametophyte.

Signal-mediated protein trafficking in plant reproduction

Changes in protein polarity similar to NTA polar accumulation in response to PT arrival have also been observed during cell-to-cell communication between the egg and sperm cells in Arabidopsis. After PT reception and release of the sperm cells, a signal from the sperm and/or the degenerated synergid causes the egg cell to secrete EGG CELL 1 (EC1) peptides that have been stored in punctate compartments in the egg cytoplasm toward the sperm cells. The sperm cells perceive the EC1 signal and, in turn, mobilize the gamete fusogen HAPLESS2/GENERATIVE CELL SPECIFIC1 (HAP2/GCS1) from a cytoplasmic compartment to the cell surface (Sprunck et al., 2012). This controlled movement of proteins that have already been translated and stored facilitates a quick response to activate the egg and sperm for fertilization. Likewise, NTA mobilization to the filiform apparatus of the synergids as the PT arrives could play a role in sending a signal to the PT that leads to the mobilization of PT proteins that allow the PT to rupture and release the sperm cells. For example, proteins that regulate the integrity of the tip of the PT could be quickly delivered after the “arrival” signal from the synergid is perceived. Recent work on the role of the pollen-expressed ANXUR1 and 2 (ANX1/2) and BUDDHA PAPER SEAL1 and 2 (BUPS1/2) receptor-like kinases in PT tip integrity support this hypothesis. During PT growth through the female tissues, RALF4 and RALF19 peptides that are secreted from PTs act as ligands for ANX1/2 and BUPS1/2 to promote tip growth, while RALF34 secreted from the female gametophyte displaces RALF4 and 19 from the receptors leading to subcellular changes that result in PT rupture (Ge et al., 2017).

Primary and secondary signals for PT rupture

Our live imaging and artificial manipulation of NTA subcellular localization data suggest a mechanism in which FER/LRE reception of a signal from the arriving PT acts as a surveillance mechanism that results in a signal transduction cascade that leads to release of a primary rupture signal from the synergid to the micropyle and also leads to trafficking of NTA from the Golgi to the filiform apparatus. At the filiform apparatus, NTA produces a secondary, or booster, rupture signal to the micropyle. We propose that in normal PT reception, a threshold of the rupture signals must be met in order for the PT to burst and release the sperm cells. The secondary signal from NTA ensures that the PTs that have passed the initial surveillance screening upon arrival will be successful in delivering their sperm cargo. This model is consistent with the incomplete penetrance of the *nta* mutant phenotype and the partial suppression of PT overgrowth in *fer* and *lre* mutants expressing faNTA (Figures 4 and 5). In *nta* mutants, the FER/LRE signaling pathway is functional and produces the primary rupture signal, which is sufficient for 70% of the PTs to burst. The remaining 30% of ovules don't reach the threshold and the PTs overgrow instead of bursting (Figure 7). Conversely, in *fer* and *lre* mutants expressing faNTA, the primary rupture signal is absent, but the secondary signal from faNTA is sufficient to reach the threshold for PT bursting in most, but not all of the ovules.

Our interspecific PT reception experiments confirmed our "primary and secondary rupture signal" hypothesis and suggest that the FER/LRE receptor complex serves as the initial surveillance system to detect arriving PTs and to invite acceptable tubes to rupture and release their sperm cells, while NTA at the filiform apparatus promotes the release of a more general rupture signal to the PT. Sequestration of NTA in the Golgi before PT arrival would allow for precise timing of release of the backup secondary rupture signal to after the FER/LRE surveillance system had permitted PT reception to proceed. This surveillance system seems to particularly important in interspecific PT reception where communication between the receptive synergid and PT is compromised, leading to PT overgrowth in response to a reduction in the strength of the synergid reaction to PT arrival and/or a higher threshold for the PT rupture signal. In contrast to intraspecific crosses where faNTA can suppress PT overgrowth in *fer* mutant ovules, in interspecific crosses, faNTA in a *fer* mutant background is not able to suppress PT overgrowth. This suggests that the surveillance function of FER is even more critical in the interaction of synergids with foreign PTs and could provide a "priming signal" to the foreign PT that allows it to respond to the faNTA-mediated signal. Alternatively, the threshold for the rupture signal in *A. lyrata* PTs could simply be higher than in *A. thaliana* PTs and the faNTA secondary signal is not

sufficient when there is no primary signal from the FER pathway. Likewise, the natural variation in *A. thaliana* reception of *A. lyrata* PTs could be related to the ability to produce sufficient amounts of the primary and secondary rupture signals from the synergids in response to PT arrival. Variation in NTA gene expression level or sequence is not correlated with natural variation in interspecific PT reception (Figure S5), indicating that other genes also play a role in this process.

Despite more than a decade of study, the identity of the signal(s) from the PT that activates the FER signaling pathway in the synergids and the identity of the PT rupture signals emitted from the synergids have remained elusive. However, the extensive literature on the FER signaling pathway in root hairs and plant-pathogen interactions gives us some clues. The FER extracellular domain interacts with several different members of the RALF family of secreted peptides (Haruta et al., 2014; Li et al., 2015; Masachis et al., 2016; Stegmann et al., 2017), therefore it is likely that the ligand that triggers the FER signal transduction pathway in synergids in response to PT arrival is also a RALF peptide. FER has also been shown to interact with pectins and has been proposed to act as monitor of cell wall damage (Feng et al., 2018). Thus, pectins could also be the ligands for FER in the filiform apparatus, allowing for a response to cell wall damage induced by the arrival of the PT.

After being attracted to the micropyle of an ovule, the PT pauses its growth in close contact with the filiform apparatus of the receptive synergid. Our model predicts that FER signal transduction results in the secretion of a primary signal that leads to PT cell wall remodeling at the tip and promotes PT rupture when the PT starts to grow again. This primary signal could be a peptide ligand that binds receptors at the PT's tip, or it could be other molecules that change the micropylar environment around the paused PT in order to affect cell wall integrity. In root hairs, FER activation by RALF1 leads to activation of plant RHO GTPase (RAC/ROP) signaling that leads to NADPH oxidase-mediated production of reactive oxygen species (ROS) (Duan et al., 2010). ROS production in the micropyle outside the synergids has also been linked to FER (Duan et al., 2014), although analysis of other PT reception mutants suggests that PT rupture may not be dependent on ROS accumulation in the micropyle (Galindo-Trigo et al., 2020). Calcium and/or calcium-regulated pathways are also candidates for the primary signal. During PT reception, the arriving PT triggers cytoplasmic calcium oscillations in the synergids (Denninger et al., 2014; Iwano et al., 2012; Ngo et al., 2014). These oscillations are dependent on active FER and LRE and are dampened in *nta* mutants. The origin and the destination of the

cytoplasmic calcium pulses in synergids are not known but it is possible that calcium could be released from internal stores into the micropyle to provide a signal to the paused PT. Our faNTA tool will be useful in future experiments to determine the contribution of NTA accumulation at the filiform apparatus to calcium signatures during PT reception and in dissecting the identities of the primary and secondary rupture signals.

Potential RLK/MLO modules in other signaling pathways

NTA and FER are both members of large gene families (Arabidopsis has 15 MLO genes and 17 CrRLK1L genes) whose members have been implicated in a variety of intercellular communication pathways in plants (Acevedo-Garcia et al., 2014; Nissen et al., 2016). While this study provides the first direct link between a CrRLK1-like receptor kinase and an MLO protein acting in the same pathway to provide redundant signals to an invading cell, we speculate that RLK-regulated trafficking of MLO proteins may be a conserved mechanism for regulating intercellular communication in other situations such as plant-pathogen interactions. For example, an interesting parallel between powdery mildew infection and PT reception is that in both cases, an MLO protein accumulates at the site of interaction with a tip-growing cell. During powdery mildew infection, active transport of proteins and lipids to penetration site leads to membrane remodeling and establishment of the extrahaustorial membrane (EHM) which separates the plant cytoplasm from the invading fungal hyphae (Huckelhoven and Panstruga, 2011). This specialized membrane is enriched in the anionic phospholipid phosphatidylinositol 4,5 bisphosphate ($PI(4,5)P_2$). Depletion of $PI(4,5)P_2$ in *phosphatidylinositol 4-phosphate 5-kinase 1/2* double mutants (*pip5k1 pip5k2*) resulted in powdery mildew resistance associated with a failure of MLO2 to accumulate at the EHM in early stages of fungal penetration (Qin et al., 2020). Both *fer* and *mlo2/6/12* mutants are resistant to powdery mildew infection (Consonni et al., 2006; Kessler et al., 2010), suggesting that the signals from the FER/MLO pathway may promote a successful interaction between the plant cell and the pathogen. Future experiments should test whether FER or related RLKs mediate asymmetric accumulation of MLO proteins as a general mechanism for intercellular communication over short time frames.

Limitations of the Study

In our study, we showed that NTA is retained in the Golgi before PT arrival and accumulates at the filiform apparatus after pollen tube arrival in the micropyle and before pollen tube rupture. The semi-*in vivo* system is challenging since it relies on both the PT and the synergid remaining healthy during lengthy live imaging experiments. Higher resolution imaging at high magnification

and shorter time intervals leads to phototoxicity in these delicate cell types. This limitation has prevented us from using photobleaching experiments to determine whether the NTA protein that accumulates at the filiform apparatus is the same protein that was retained in the Golgi or newly translated protein.

Acknowledgements

We thank Lindsey Berebitsky and Daniel Cabada Gomez for technical assistance and Dr. Ravi Palanivelu, Dr. Subramanian Sankaranarayanan, and Kessler lab members for helpful discussions and comments. We thank the anonymous reviewers for their comments and suggestions to improve the manuscript. This work was supported by funds from NSF IOS-1733865 to SAK, Purdue University Start-up funds to SAK, and a grant from the Oklahoma Center for the Advancement of Science and Technology #PS14-008 to SAK. Spinning disk confocal microscopy in the Staiger laboratory was supported, in part, by an award from the Office of Science at the US Department of Energy, Physical Biosciences Program, under contract number DE-FG02-09ER15526 to CJS.

Author Contributions

YJ, JY, DSJ, and SAK conceived and designed the experiments. YJ, JY, DSJ, and WZ performed the experiments. YJ performed the artificial NTA manipulation experiments and genetic analysis in mutant backgrounds and interspecific crosses. JY performed the semi-*in vivo* live imaging experiments. YJ, JY, DSJ, and SAK analyzed the data. YJ, JY, DSJ, and SAK wrote the manuscript, and all authors revised and approved the final manuscript.

Declaration of Interests

The authors declare no competing interests.

Main Figure Titles and Legends

Figure 1. NTA-GFP accumulates at the filiform apparatus as the PT approaches.
(A) Diagram of a mature *Arabidopsis thaliana* ovule and embryo sac. Syn, synergid; FA, filiform apparatus; CC, central cell; An, antipodal cells. (B and C) Live imaging of PT reception using NTA-GFP labeled synergids (green signal) and ACA9::DsRed PTs (magenta signal). (B) Polar NTA-GFP accumulation at the FA occurred in ovules that attracted a PT (ovules with yellow stars), while polar NTA-GFP accumulation did not occur in ovules without PT attraction (ovules with white stars). Bar = 50 μm. (C) Time-lapse imaging of NTA-GFP accumulation during PT reception. Bar = 50 μm. (D) Quantification of NTA-GFP signal from (C) along the length of the synergid from chalazal end (0 μm) to FA end (33 μm) at 0 min, 25 min, 50 min, 75 min, and 100 min timepoints, respectively. Error bars were calculated from the average value of the same

length line at five parallel position within the synergid. (E) 6 more examples of the quantification of NTA-GFP signal along the length of synergids after PT arrival. (F) Quantification of the percentage of ovules with different NTA accumulation patterns under the same imaging conditions. n represents ovule numbers observed.

Figure 2. A Golgi marker is randomly distributed throughout synergids during PT reception.
(A) NTA-GFP (green signal) and Golgi-mCherry signals (magenta signal) are evenly distributed along the length of the synergid and co-localized within synergids before PT arrival. Bar = 30 μm. (B) After PT arrival, NTA-GFP accumulated at the FA, but Golgi-mCherry did not accumulate at the FA. Bar = 30 μm. (C) Live imaging of Golgi-mCherry during PT reception with Lat52::GFP labeled PTs. Bar = 50 μm. (D) Quantification of Golgi-mCherry signal along the length of synergids shown in (C) before and after PT arrival. Error bars calculated based on the average intensity value of the same length line at five parallel position within the synergid.

Figure 3. Accumulation of NTA at the filiform apparatus is necessary and sufficent for PT reception.
(A-E) Diagrams and subcellular localization patterns of MYB98 promoter driven MLO-GFP variants (green signal) in synergids of mature virgin ovules stained with FM4-64 (magenta signal) to reveal the outline of the synergid and the filiform apparatus (diffuse magenta signal). Light yellow rectangles in the diagrams indicate plasma membrane. Graphs in each panel show quantification of the GFP intensity of the MLO variants along the length of the synergids. Error bars: the average value of the same length line at five parallel position within the synergid. Bars = 10 μm. CaMBD: Calmodulin binding domain. (F) Percentage of ovules showing MLO-GFP signal throughout the synergids (100% of length), in the FA only (20% of length) and the region surrounding and including the FA (40% of length). (G) Scatter plot of unfertilized ovule percentages in homozygous plants of pMYB98::MLO-GFP in *nta-1* mutants to assess the ability of the MLO-GFP constructs to complement *nta-1*. Each dot represents the average of 5 siliques from one individual plant. Ws-2, Wassilewskija-2. Significance was determined by a one-way ANOVA with Tukey test (****, $P \leqslant 0.0001$; ***, $P \leqslant 0.001$; **, $P \leqslant 0.01$; and ns, $P > 0.05$).

Figure 4. faNTA bypasses FER signaling pathway in PT reception.
(A) Diagram of side view of synergids. (B) faNTA-GFP is localized to the filiform apparatus in *fer-1* ovules before PT arrival. Bar = 10 μm. (C) NTA-GFP is retained in the Golgi in unfertilized *fer-1* ovules. Bar = 10 μm. (D) Opened siliques from *fer-1* 10 days after pollination. Black stars indicate unfertilized ovules. Bar = 2 mm. (E) Opened siliques from *faNTA;fer-1* 10 days after pollination. Black stars indicate unfertilized ovules. Bar = 2 mm. (F) faNTA suppresses the infertility phenotype of *fer-1*. Significance was determined by a one-way ANOVA with Tukey test (****, $P \leqslant 0.0001$; ns, $P > 0.05$). (G) PT overgrowth in *faNTA;fer-1* is reduced compared to *fer-1*. PT OG/S represents PT overgrowth per silique. Significance was determined by a student's *t* test (****, $P \leqslant 0.0001$). (H) PT overgrowth in *faNTA;fer-1* ovules. Arrowheads indicates PT overgrowth in unfertilized ovules, and arrow indicates normal PT reception in a fertilized ovule. Bar = 50 μm.

Figure 5. faNTA suppresses *lre-7* infertility and does not suppress *tun-2/+* or the pollen triple *myb* mutant.
(A) faNTA-GFP is localized to the filiform apparatus in unpollinated *lre-7* ovules. Bar = 10 μm. (B) faNTA-GFP is localized to the filiform apparatus in *tun-2/+* unpollinated ovules. Bar = 10 μm. (C-

F) Opened siliques showing plant fertility from genotypes *lre-7* (C), *faNTA;lre-7* (D), *tun-2/+* (E), and *faNTA;tun-2/+* (F). Black stars indicate unfertilized ovules. Bars = 2 mm. (G) faNTA suppresses the infertility phenotype of *lre-7* (blue colors) and faNTA does not suppress *tun-2/+* infertility (magenta colors). Significance was determined by a one-way ANOVA with Tukey test (****, $P \leqslant 0.0001$; ns, $P > 0.05$). (H) The role of faNTA in PT reception is independent of triple MYBs in the pollen. Significance was determined by a student's *t* test (ns, $P > 0.05$).

Figure 6. NTA promotes interspecific PT reception.
(A) Effects of synergid expression of MLO variants on PT reception in interspecific crosses with *A. lyrata* pollen. The MLO constructs are in the *nta-1* background. (B) faNTA's suppression of *A. lyrata* PT overgrowth is FER-dependent. (C) faNTA and NTA reduce PT overgrowth rate in the Lp2-2 accession. Significance was determined by a one-way ANOVA with Tukey test for (A) and (B) and with Dunnett test for (C) (****, $P \leqslant 0.0001$; ***, $P \leqslant 0.001$; **, $P \leqslant 0.01$; *, $P \leqslant 0.05$; and ns, $P > 0.05$). (D) Aniline blue staining showing PT overgrowth (white stars) in Lp2-2, hemizygous faNTA in Lp2-2; homozygous faNTA in Lp2-2, and hemizygous NTA in Lp2-2. Bar = 500 μm.

Figure 7. Model for NTA function in PT reception.
(A) FER/LRE activation by an arriving PT (PT) leads to the release of primary rupture signals (blue dots), while trafficking of NTA to the filiform apparatus (faNTA) leads to the release of secondary rupture signals (green dots) to ensure that all compatible PTs burst in *A. thaliana*. (B-D) Insufficient primary or secondary signals in mutants leads to higher rates of PT overgrowth (PT OG) that can be rescued with artificial faNTA. (E-H) In interspecific crosses, *A. thaliana* FER/LRE signaling is compromised in response to *A. lyrata* PTs, but faNTA can boost the ability of foreign PTs to burst as long as FER activity is also present.

STAR METHODS

RESOURCE AVAILABILITY

Lead Contact

Further information and requests for resources and reagents should be directed to and will be fulfilled by the Lead Contact, Sharon A. Kessler (sakessler@purdue.edu).

Materials Availability

All constructs and plant lines developed for this project are available upon request to the Lead Contact.

Data and Code Availability

This study did not generate any unique datasets or code. Any additional information required to reanalyze the data reported in this paper is available from the lead contact upon request.

EXPERIMENTAL MODEL AND SUBJECT DETAILS

Plant Materials and Growth Conditions

All seeds were surface-sterilized before plating.
Arabidopsis thaliana ecotypes Col-0, Ws-2, L*er*, and Lp2-2 were used as wild-type controls. Seeds from these backgrounds were plated on ½ Murashige and Skoog (MS) medium with or without antibiotics. For transgenic screening, the plates were supplemented with hygromycin to a final concentration of 20 mg/L. For *tun-2/+* and *lre-7/+* segregation experiments, the plates were supplemented with Basta to a final concentration of 10 mg/L. For *fer-1/+* segregation experiments, seeds were plated on full-strength MS medium with 50 mg/L kanamycin. Seeds were stratified at 4ºC for 2 days before being transferred to the growth chamber (22ºC, 16 hour-light/8 hour-dark cycle). After 10 days, seedlings were transplanted to soil with the exception that homozygous *fer-1* seeds were put on soil directly.
Arabidopsis thaliana ecotypes Lz-0, Ga-0, Sha, Mrk-0, Rmx-A02, Sorbo, Pu2-23, Br-0, Van-0, Gu-0, Uod-1, Kin-0, HR-5, Se-0, Ei-2, Ts-1, Mz-0, Lp2-2, Ra-0, Sq-8, and Kz-9 were plated on ½ MS plates, stratified at 4ºC for 2 days, transferred to the growth chamber for 10 days, vernalized at 4 ºC for 4 weeks, transplanted to soil, and grown in the same chamber.
Arabidopsis lyrata seeds were plated on ½ MS plates, stratified at 4ºC for 10 days, transferred to the growth chamber for 10 days, transplanted to soil, and grown in the same chamber.
Nicotiana benthamiana seeds were sown directly on soil and grown under the same conditions as Arabidopsis.

METHOD DETAILS

Live Imaging of Pollination Using a Semi-*in vivo* PT Guidance Assay

The semi-*in vivo* system of PT reception was modified from (Palanivelu and Preuss, 2006). Approximately 150 µL of pollen germination media (5 mM KCl, 1 mM $MgSO_4$, 0.01% (w/v) H_3BO_3, 5 mM $CaCl_2$, 20% sucrose, 1.5% low melting point agarose, and adjusted pH to 7.5 with KOH) was poured into a Glass Bottom Culture Petri Dish (MatTek Corporation, P35G-1.0-20-C) and spread out using a pipette. Pistils were emasculated and 2 d later were hand pollinated with *ACA9::DsRed* or *Lat52::GFP* pollen and returned to the growth chamber. Approximately 1 h after pollination, pistils were removed from plants and placed on double sided tape on a glass slide. Stigmas were cut using single-sided razor blade and placed on pollen germination media using forceps. 8-10 ovules were arranged around the cut style and the petri dish was returned to the growth chamber. After 4-6 h, PTs grew through the stigma and style and emerged near the ovules. Imaging commenced when the PTs approached ovules. Time-lapse images were acquired at 5 min intervals by spinning disk confocal microscopy using an Andor Revolution XD platform with a Yokogawa CSU-X1-A1 scanner unit mounted on an Olympus IX-83 microscope and a 20X/0.5 NA objective (Olympus). An Andor iXon Ultra 897BV EMCCD camera was used to capture GFP fluorescence (488-nm excitation) and red fluorescent protein (DsRed or mCherry) fluorescence (561-nm excitation). For all live imaging experiments, the digitizer for both 488-nm and 561-nm laser was 16-bit (17MHz, EM Gain), the gain value was 200 and the exposure time was 100.0 ms. The laser intensity was 20.0 for the 488-nm laser and 15.0 for the 561-nm laser.
For each experimental condition, at least 60 ovules were imaged over the time course from PT approaching the ovule to completion of PT reception (PT rupture to release the sperm cells). Neighboring ovules that did not attract PTs were imaged at the same time and served as controls for photoxicity.

Confocal laser scanning microscopy (CLSM)

Ovules from MLO-variant-GFP lines were dissected (valves removed) and retained on the septum for analysis of GFP localization or distribution on a CLSM. FM4-64 staining was performed according to the protocol described in (Jones et al., 2017). Freshly dissected ovules were incubated in 20 µM FM4-64 in PIPES buffer (50 mM PIPES, 5 mM EGTA, and 1 mM $MgSO_4$ at pH 6.8) for 20 min on a slide on ice in a humid chamber. Coverslips were put on the samples right before imaging. Images were taken using either a Nikon A1Rsi inverted confocal microscope according to (Yuan and Kessler, 2019) or a Leica Zeiss LSM 880 upright confocal microscope.

Cloning and Generation of Transgenic Lines

PCR amplification with Q5 High-Fidelity DNA Polymerase were used to generate the following constructs in this study with Gateway cloning. Entry vectors pDONR207-NTA and pDONR207-MLO1, expression vectors 35S::NTA-GFP, 35S::MLO1-GFP, and 35S::NTA-Cer3 were described previously (Jones and Kessler, 2017; Jones et al., 2017; Kessler et al., 2010). Two fragments of *NTA* and *MLO1* were amplified with pDONR207-NTA and pDONR207-MLO1 as templates and with primer pairs NTA-FattB1 +NTA-R19 and MLO1-F + MLO1-RattB2 (See all primer sequences in Table S2). The two fragments were purified and pasted together (named faNTA) with overlaps using a PCR-pasting protocol. The faNTA entry construct was generated via BP reaction with pDONR207 as a backbone. faNTA entry vector was recombined via LR reaction into the pMDC83 with MYB98 promoter (Muller et al., 2016) to generate pMYB98::faNTA-GFP.

The **NTA-GFP-RNIKCD entry vector** was generated using the full-length expression vector of $MYB98_{pro}$::NTA-GFP as template. Two separate fragments of *NTA* and *GFP-RNIKCD-1* were amplified with two pairs of primers: NTA-FattB1 + NTA-Gly5-GFP-R and NTA-Gly5-GFP-F + GFP-RNIKCD-RattB2. The two fragments were purified and pasted together with overlaps using a PCR-pasting protocol. The **faNTA-GFP-RNIKCD entry vector** was generated using the full-length expression vector of $MYB98_{pro}$::faNTA-GFP as template and two fragments of *faNTA* and *GFP-RNIKCD-2* were amplified using the two pairs of primers: NTA-FattB1 + MLO1-Gly5-GFP-R and MLO1-Gly5-GFP-F + GFP-RNIKCD-RattB2. The two fragments were purified and pasted together with overlaps using a PCR-pasting protocol. The **MLO1-GFP-RNIKCD entry vector** The entry vectors was generated using the full-length expression vector of 35S::MLO1-GFP as template and two fragments of *MLO1* and *GFP-RNIKCD-2* were amplified using the two pairs of primers: MLO1-FattB1 + MLO1-Gly5-GFP-R and MLO1-Gly5-GFP-F + GFP-RNIKCD-RattB2. The two fragments were purified and pasted together with overlaps using a PCR-pasting protocol. NTA-GFP-RNIKCD and faNTA-GFP-RNIKCD were recombined via LR reactions into the pMDC32 with MYB98 promoter and pMDC32 with FER promoter for synergid expression and tobacco leaf transient expression, respectively. MLO1-GFP-RNIKCD was recombined via LR reactions into the pMDC32 with FER promoter for tobacco leaf transient expression.

For *nta-1* complementation assay and co-localization analyses, expression vectors were transformed into the *Agrobacterium tumefaciens* strain GV3101 and transformed into the *nta-1* mutant background and the Col-0 background with Golgi marker (pLRE::Man49-mCherry) via the floral-dip method (Bent, 2006). Hygromycin was used to screen stable transgenic lines. Homozygous T2 to T4 lines were used in *nta-1* complementation assay and co-localization imaging in the synergid was done in a T1 or T2 analysis. The pNTA::NTA-GFP construct described in (Kessler et al., 2010) was introduced into the *lre-7* background by floral dip method. The pMYB98::NTA-GFP was introduced to *fer-1* by floral dip method. pMYB98::faNTA-GFP was introduced to *fer-1*, *lre-7*, and *tun-2/+* by crosses.

***nta-1* Complementation Assays**

At least 2 independent insertion lines for each construct were taken to the T2 generation and screened for homozygosity using fluorescence microscopy to ensure transgene expression in synergids of every ovule. Counts of unfertilized ovules and fertilized ovules were done from the 6th silique to the 10th silique on the main branch to determine plant fertility. Unfertilized vs. fertilized ovule counts from self-pollinated flowers were assessed in five plants of each insertion line and compared to *nta-1*, Wassilewskija (Ws-2; wildtype), and the previously published full-length NTA (pMYB98::NTA-GFP in *nta-1* background)(Jones et al., 2017). Ovule counts were statistically analyzed using Prism with significance determined using one-way ANOVA with Tukey test.

Aniline blue staining

Pistils were pollinated two days after emasculation. After another two days, siliques were fixed overnight in fixative solution (ethanol: acetic acid=9:1) at 4^{o}C. Samples were then rehydrated in 70% ethanol, 50 ethanol, and 30% ethanol for 5 minutes in each solution in room temperature. Siliques were put in chloral hydrate for 5 minutes at 60^{o}C, and then washed in 100 mM phosphate buffer pH 7.0. Siliques were then softened in 5 M NaOH for 10 minutes at 60^{o}C. After 2 washes with 100 mM phosphate buffer, samples were mounted in 0.1% aniline blue solution for imaging. Aniline blue staining samples were visualized by the DAPI filter on an inverted Nikon Eclipse Ti2-E epifluorescence microscope.

Quantitative Real-time PCR
Total RNA was extracted from newly opened stage 13 flowers using E.Z.N.A Plant RNA Kit (Omega, USA), after which 800 ng of total RNA was reverse-transcript with SuperScript™ III First-Strand Synthesis System (Invitrogen) according to the manufacturer's instructions. Real-time qPCR was performed on a StepOnePlus™ System using *Power* SYBR™ Green PCR Master Mix. The PCR conditions were 95°C for 15 s, followed by 45 cycles of 95°C for 5 s, 55°C for 20 s, and 72°C for 30 s. Three technical replicates were performed with each cDNA template. The results were normalized using *ACT2*. The primers used for real-time PCR are listed in Table S2.

Imaging Processing
All images were processed in Adobe Photoshop (Version 19.1.3) and Adobe Illustrator (Version 22.1).

Video processing
Images were adjusted for brightness and contrast and cropped using Fiji (Version 2.0.0). QuickTime Player (Version 10.5) was used for adding movie time and time-lapse analyses. Split screen videos were processed in Adobe Premiere Pro (Version 14.0.4).

QUANTIFICATION AND STATISTICAL ANALYSIS

Quantification of fluorescence signal intensity
Two-channel images of all live-imaging experiments were adjusted for brightness and contrast using Fiji (Schindelin et al., 2012). The adjustments were done consistently for all the images. Raw image data was analyzed with NIS-Elements software (Ver. 5.02) to measure the fluorescence signal intensity. A line that spanned from the chalazal end to the filiform apparatus end of the synergid was used for the signal intensity measurements. For a more accurate representation of the total area of the synergid, signal intensities were recorded along the same length line at five parallel positions within the synergid. Finally, all the measurement data were output as Excel files. Graphs and statistical analysis were performed with Prism software (Version 9.1.0, www.graphpad.com).

Statistical Analysis
Statistical analysis was examined either by Student's *t*-test or by one-way ANOVA with Tukey's multiple comparisons test or Dunnett's multiple comparisons test using the GraphPad Prism 9 software.

References

Acevedo-Garcia, J., Kusch, S., and Panstruga, R. (2014). Magical mystery tour: MLO proteins in plant immunity and beyond. New Phytol *204*, 273-281.

Bent, A. (2006). Arabidopsis thaliana floral dip transformation method. Methods Mol Biol *343*, 87-103.

Bhat, R.A., Miklis, M., Schmelzer, E., Schulze-Lefert, P., and Panstruga, R. (2005). Recruitment and interaction dynamics of plant penetration resistance components in a plasma membrane microdomain. Proc Natl Acad Sci USA *102*, 3135-3140.

Capron, A., Gourgues, M., Neiva, L.S., Faure, J.E., Berger, F., Pagnussat, G., Krishnan, A., Alvarez-Mejia, C., Vielle-Calzada, J.P., Lee, Y.R*., et al.* (2008). Maternal control of male-gamete delivery in Arabidopsis involves a putative GPI-anchored protein encoded by the LORELEI gene. Plant Cell *20*, 3038-3049.

Consonni, C., Humphry, M.E., Hartmann, H.A., Livaja, M., Durner, J., Westphal, L., Vogel, J., Lipka, V., Kemmerling, B., Schulze-Lefert, P*., et al.* (2006). Conserved requirement for a plant host cell protein in powdery mildew pathogenesis. Nat Genet *38*, 716-720.

Denninger, P., Bleckmann, A., Lausser, A., Vogler, F., Ott, T., Ehrhardt, D.W., Frommer, W.B., Sprunck, S., Dresselhaus, T., and Grossmann, G. (2014). Male-female communication triggers calcium signatures during fertilization in Arabidopsis. Nat Commun *5*, 4645.
Drews, G.N., and Yadegari, R. (2002). Development and function of the angiosperm female gametophyte. Annu Rev Genet *36*, 99-124.
Duan, Q., Kita, D., Johnson, E.A., Aggarwal, M., Gates, L., Wu, H.M., and Cheung, A.Y. (2014). Reactive oxygen species mediate pollen tube rupture to release sperm for fertilization in Arabidopsis. Nat Commun *5*, 3129.
Duan, Q., Kita, D., Li, C., Cheung, A.Y., and Wu, H.M. (2010). FERONIA receptor-like kinase regulates RHO GTPase signaling of root hair development. Proc Natl Acad Sci USA *107*, 17821-17826.
Escobar-Restrepo, J.M., Huck, N., Kessler, S., Gagliardini, V., Gheyselinck, J., Yang, W.C., and Grossniklaus, U. (2007). The FERONIA receptor-like kinase mediates male-female interactions during pollen tube reception. Science *317*, 656-660.
Feng, W., Kita, D., Peaucelle, A., Cartwright, H.N., Doan, V., Duan, Q., Liu, M.C., Maman, J., Steinhorst, L., Schmitz-Thom, I.*, et al.* (2018). The FERONIA Receptor Kinase Maintains Cell-Wall Integrity during Salt Stress through Ca(2+) Signaling. Curr Biol *28*, 666-675 e665.
Galindo-Trigo, S., Blanco-Tourinan, N., DeFalco, T.A., Wells, E.S., Gray, J.E., Zipfel, C., and Smith, L.M. (2020). CrRLK1L receptor-like kinases HERK1 and ANJEA are female determinants of pollen tube reception. EMBO Rep *21*, e48466.
Gao, C., Yu, C.K., Qu, S., San, M.W., Li, K.Y., Lo, S.W., and Jiang, L. (2012). The Golgi-localized Arabidopsis endomembrane protein12 contains both endoplasmic reticulum export and Golgi retention signals at its C terminus. Plant Cell *24*, 2086-2104.
Ge, Z., Bergonci, T., Zhao, Y., Zou, Y., Du, S., Liu, M.C., Luo, X., Ruan, H., Garcia-Valencia, L.E., Zhong, S.*, et al.* (2017). Arabidopsis pollen tube integrity and sperm release are regulated by RALF-mediated signaling. Science *358*, 1596-1600.
Geldner, N., Denervaud-Tendon, V., Hyman, D.L., Mayer, U., Stierhof, Y.D., and Chory, J. (2009). Rapid, combinatorial analysis of membrane compartments in intact plants with a multicolor marker set. Plant J *59*, 169-178.
Hamamura, Y., Nagahara, S., and Higashiyama, T. (2012). Double fertilization on the move. Curr Opin Plant Biol *15*, 70-77.
Hamamura, Y., Nishimaki, M., Takeuchi, H., Geitmann, A., Kurihara, D., and Higashiyama, T. (2014). Live imaging of calcium spikes during double fertilization in Arabidopsis. Nat Commun *5*, 4722.
Hamamura, Y., Saito, C., Awai, C., Kurihara, D., Miyawaki, A., Nakagawa, T., Kanaoka, M.M., Sasaki, N., Nakano, A., Berger, F.*, et al.* (2011). Live-cell imaging reveals the dynamics of two sperm cells during double fertilization in Arabidopsis thaliana. Curr Biol *21*, 497-502.
Haruta, M., Sabat, G., Stecker, K., Minkoff, B.B., and Sussman, M.R. (2014). A peptide hormone and its receptor protein kinase regulate plant cell expansion. Science *343*, 408-411.
Huang, B.-Q., and Russell, S.D. (1992). Female Germ Unit: Organization, Isolation, and Function. *140*, 233-293.
Huang, J., Ju, Y., Wang, X., Zhang, Q., and Sodmergen (2015). A one-step rectification of sperm cell targeting ensures the success of double fertilization. J Integr Plant Biol *57*, 496-503.

Huck, N., Moore, J.M., Federer, M., and Grossniklaus, U. (2003). The Arabidopsis mutant feronia disrupts the female gametophytic control of pollen tube reception. Development *130*, 2149-2159.
Huckelhoven, R., and Panstruga, R. (2011). Cell biology of the plant-powdery mildew interaction. Curr Opin Plant Biol *14*, 738-746.
Iwano, M., Ngo, Q.A., Entani, T., Shiba, H., Nagai, T., Miyawaki, A., Isogai, A., Grossniklaus, U., and Takayama, S. (2012). Cytoplasmic Ca2+ changes dynamically during the interaction of the pollen tube with synergid cells. Development *139*, 4202-4209.
Johnson, M.A., Harper, J.F., and Palanivelu, R. (2019). A Fruitful Journey: Pollen Tube Navigation from Germination to Fertilization. Annu Rev Plant Biol *70*, 809-837.
Jones, D.S., and Kessler, S.A. (2017). Cell type-dependent localization of MLO proteins. Plant Signal Behav *12*, e1393135.
Jones, D.S., Liu, X., Willoughby, A.C., Smith, B.E., Palanivelu, R., and Kessler, S.A. (2018). Cellular distribution of secretory pathway markers in the haploid synergid cells of Arabidopsis thaliana. Plant J *94*, 192-202.
Jones, D.S., Yuan, J., Smith, B.E., Willoughby, A.C., Kumimoto, E.L., and Kessler, S.A. (2017). MILDEW RESISTANCE LOCUS O Function in Pollen Tube Reception Is Linked to Its Oligomerization and Subcellular Distribution. Plant Physiol *175*, 172-185.
Kessler, S.A., and Grossniklaus, U. (2011). She's the boss: signaling in pollen tube reception. Curr Opin Plant Biol *14*, 622-627.
Kessler, S.A., Shimosato-Asano, H., Keinath, N.F., Wuest, S.E., Ingram, G., Panstruga, R., and Grossniklaus, U. (2010). Conserved molecular components for pollen tube reception and fungal invasion. Science *330*, 968-971.
Leshem, Y., Johnson, C., and Sundaresan, V. (2013). Pollen tube entry into the synergid cell of Arabidopsis is observed at a site distinct from the filiform apparatus. Plant Reprod *26*, 93-99.
Leydon, A.R., Beale, K.M., Woroniecka, K., Castner, E., Chen, J., Horgan, C., Palanivelu, R., and Johnson, M.A. (2013). Three MYB transcription factors control pollen tube differentiation required for sperm release. Curr Biol *23*, 1209-1214.
Li, C., Yeh, F.L., Cheung, A.Y., Duan, Q., Kita, D., Liu, M.C., Maman, J., Luu, E.J., Wu, B.W., Gates, L.*, et al.* (2015). Glycosylphosphatidylinositol-anchored proteins as chaperones and co-receptors for FERONIA receptor kinase signaling in Arabidopsis. Elife *4*, e06587.
Lindner, H., Kessler, S.A., Muller, L.M., Shimosato-Asano, H., Boisson-Dernier, A., and Grossniklaus, U. (2015). TURAN and EVAN mediate pollen tube reception in Arabidopsis Synergids through protein glycosylation. PLoS Biol *13*, e1002139.
Liu, X., Castro, C., Wang, Y., Noble, J., Ponvert, N., Bundy, M., Hoel, C., Shpak, E., and Palanivelu, R. (2016). The Role of LORELEI in Pollen Tube Reception at the Interface of the Synergid Cell and Pollen Tube Requires the Modified Eight-Cysteine Motif and the Receptor-Like Kinase FERONIA. Plant Cell *28*, 1035-1052.
Mansfield, S.G., Briarty, L.G., and Erni, S. (1991). Early embryogenesis in Arabidopsis thaliana. I. The mature embryo sac. Canadian Journal of Botany *69*, 447-460.
Masachis, S., Segorbe, D., Turra, D., Leon-Ruiz, M., Furst, U., El Ghalid, M., Leonard, G., Lopez-Berges, M.S., Richards, T.A., Felix, G.*, et al.* (2016). A fungal pathogen secretes plant alkalinizing peptides to increase infection. Nat Microbiol *1*, 16043.

Muller, L.M., Lindner, H., Pires, N.D., Gagliardini, V., and Grossniklaus, U. (2016). A subunit of the oligosaccharyltransferase complex is required for interspecific gametophyte recognition in Arabidopsis. Nat Commun *7*, 10826.
Naramoto, S. (2017). Polar transport in plants mediated by membrane transporters: focus on mechanisms of polar auxin transport. Curr Opin Plant Biol *40*, 8-14.
Ngo, Q.A., Vogler, H., Lituiev, D.S., Nestorova, A., and Grossniklaus, U. (2014). A Calcium Dialog Mediated by the FERONIA Signal Transduction Pathway Controls Plant Sperm Delivery. Dev Cell *29*, 491-500.
Nissen, K.S., Willats, W.G.T., and Malinovsky, F.G. (2016). Understanding CrRLK1L Function: Cell Walls and Growth Control. Trends Plant Sci *21*, 516-527.
Okuda, S., Tsutsui, H., Shiina, K., Sprunck, S., Takeuchi, H., Yui, R., Kasahara, R.D., Hamamura, Y., Mizukami, A., Susaki, D*., et al.* (2009). Defensin-like polypeptide LUREs are pollen tube attractants secreted from synergid cells. Nature *458*, 357-361.
Palanivelu, R., and Preuss, D. (2006). Distinct short-range ovule signals attract or repel Arabidopsis thaliana pollen tubes in vitro. BMC Plant Biol *6*, 7.
Petrasek, J., Mravec, J., Bouchard, R., Blakeslee, J.J., Abas, M., Seifertova, D., Wisniewska, J., Tadele, Z., Kubes, M., Covanova, M*., et al.* (2006). PIN proteins perform a rate-limiting function in cellular auxin efflux. Science *312*, 914-918.
Qin, L., Zhou, Z., Li, Q., Zhai, C., Liu, L., Quilichini, T.D., Gao, P., Kessler, S.A., Jaillais, Y., Datla, R*., et al.* (2020). Specific Recruitment of Phosphoinositide Species to the Plant-Pathogen Interfacial Membrane Underlies Arabidopsis Susceptibility to Fungal Infection. Plant Cell *32*, 1665-1688.
Rotman, N., Rozier, F., Boavida, L., Dumas, C., Berger, F., and Faure, J.E. (2003). Female control of male gamete delivery during fertilization in Arabidopsis thaliana. Curr Biol *13*, 432-436.
Salanenka, Y., Verstraeten, I., Lofke, C., Tabata, K., Naramoto, S., Glanc, M., and Friml, J. (2018). Gibberellin DELLA signaling targets the retromer complex to redirect protein trafficking to the plasma membrane. Proc Natl Acad Sci USA *115*, 3716-3721.
Schindelin, J., Arganda-Carreras, I., Frise, E., Kaynig, V., Longair, M., Pietzsch, T., Preibisch, S., Rueden, C., Saalfeld, S., Schmid, B*., et al.* (2012). Fiji: an open-source platform for biological-image analysis. Nat Methods *9*, 676-682.
Sprunck, S., Rademacher, S., Vogler, F., Gheyselinck, J., Grossniklaus, U., and Dresselhaus, T. (2012). Egg cell-secreted EC1 triggers sperm cell activation during double fertilization. Science *338*, 1093-1097.
Stegmann, M., Monaghan, J., Smakowska-Luzan, E., Rovenich, H., Lehner, A., Holton, N., Belkhadir, Y., and Zipfel, C. (2017). The receptor kinase FER is a RALF-regulated scaffold controlling plant immune signaling. Science *355*, 287-289.
Takeuchi, H., and Higashiyama, T. (2016). Tip-localized receptors control pollen tube growth and LURE sensing in Arabidopsis. Nature *531*, 245-248.
Underwood, W., Ryan, A., and Somerville, S.C. (2017). An Arabidopsis Lipid Flippase Is Required for Timely Recruitment of Defenses to the Host-Pathogen Interface at the Plant Cell Surface. Mol Plant *10*, 805-820.
Underwood, W., and Somerville, S.C. (2013). Perception of conserved pathogen elicitors at the plasma membrane leads to relocalization of the Arabidopsis PEN3 transporter. Proc Natl Acad Sci USA *110*, 12492-12497.

Viotti, C., Bubeck, J., Stierhof, Y.D., Krebs, M., Langhans, M., van den Berg, W., van Dongen, W., Richter, S., Geldner, N., Takano, J.*, et al.* (2010). Endocytic and secretory traffic in Arabidopsis merge in the trans-Golgi network/early endosome, an independent and highly dynamic organelle. Plant Cell *22*, 1344-1357.
Wang, T., Liang, L., Xue, Y., Jia, P.F., Chen, W., Zhang, M.X., Wang, Y.C., Li, H.J., and Yang, W.C. (2016). A receptor heteromer mediates the male perception of female attractants in plants. Nature *531*, 241-244.
Yu, M., Li, R., Cui, Y., Chen, W., Li, B., Zhang, X., Bu, Y., Cao, Y., Xing, J., Jewaria, P.K.*, et al.* (2020). The RALF1-FERONIA interaction modulates endocytosis to mediate control of root growth in Arabidopsis. Development *147*, dev189902.
Yuan, J., and Kessler, S.A. (2019). A genome-wide association study reveals a novel regulator of ovule number and fertility in Arabidopsis thaliana. PLoS Genet *15*, e1007934.

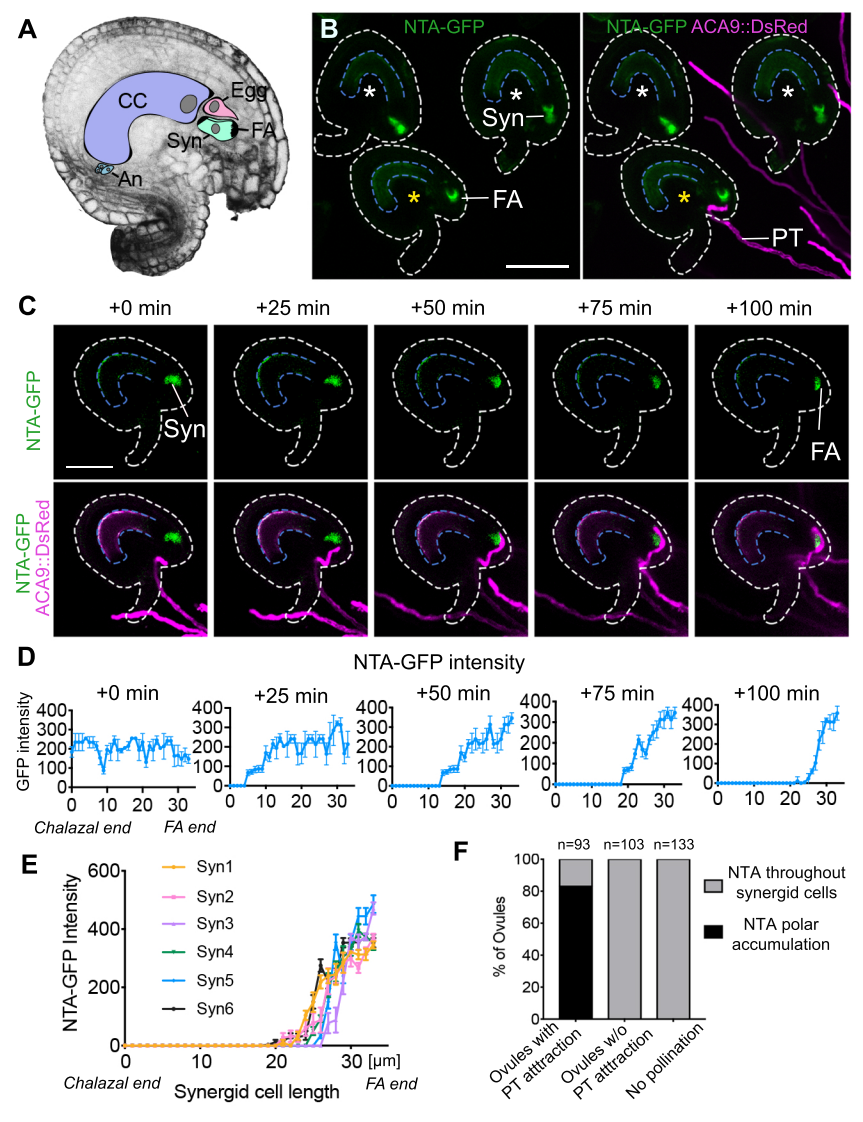
A
CC
Egg
FA
Syn
An
B
NTA-GFP
NTA-GFP ACA9::DsRed
Syn
FA
PT
C
+0 min
+25 min
+50 min
+75 min
+100 min
NTA-GFP
Syn
FA
NTA-GFP
ACA9::DsRed
D
NTA-GFP intensity
+0 min
+25 min
+50 min
+75 min
+100 min
GFP intensity
Chalazal end
FA end
E
NTA-GFP Intensity
Syn1
Syn2
Syn3
Syn4
Syn5
Syn6
Chalazal end
Synergid cell length
FA end
F
n=93
n=103
n=133
% of Ovules
NTA throughout synergid cells
NTA polar accumulation
Ovules with PT atttraction
Ovules w/o PT atttraction
No pollination

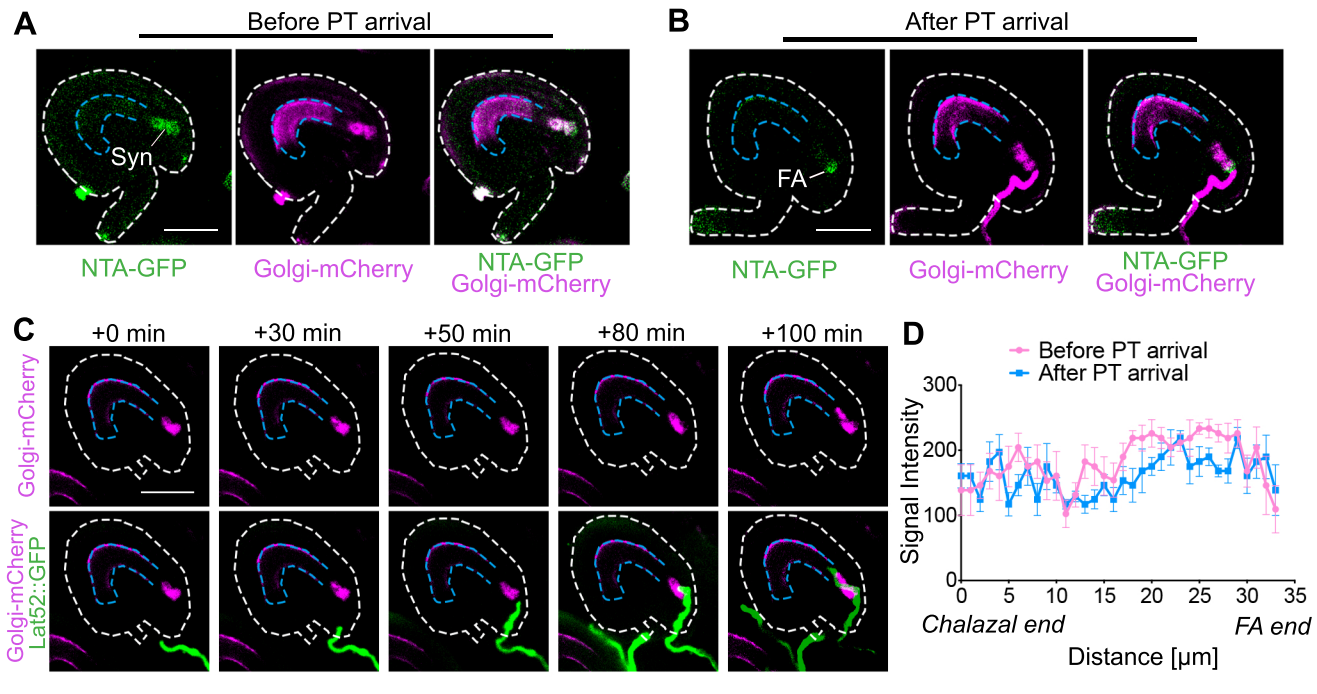
A
Before PT arrival
Syn
NTA-GFP
Golgi-mCherry
NTA-GFP
Golgi-mCherry
B
After PT arrival
FA
NTA-GFP
Golgi-mCherry
NTA-GFP
Golgi-mCherry
C
+0 min
+30 min
+50 min
+80 min
+100 min
Golgi-mCherry
Golgi-mCherry
Lat52::GFP
D
Before PT arrival
After PT arrival
Signal Intensity
300
200
100
0
0
5
10
15
20
25
30
35
Chalazal end
FA end
Distance [μm]

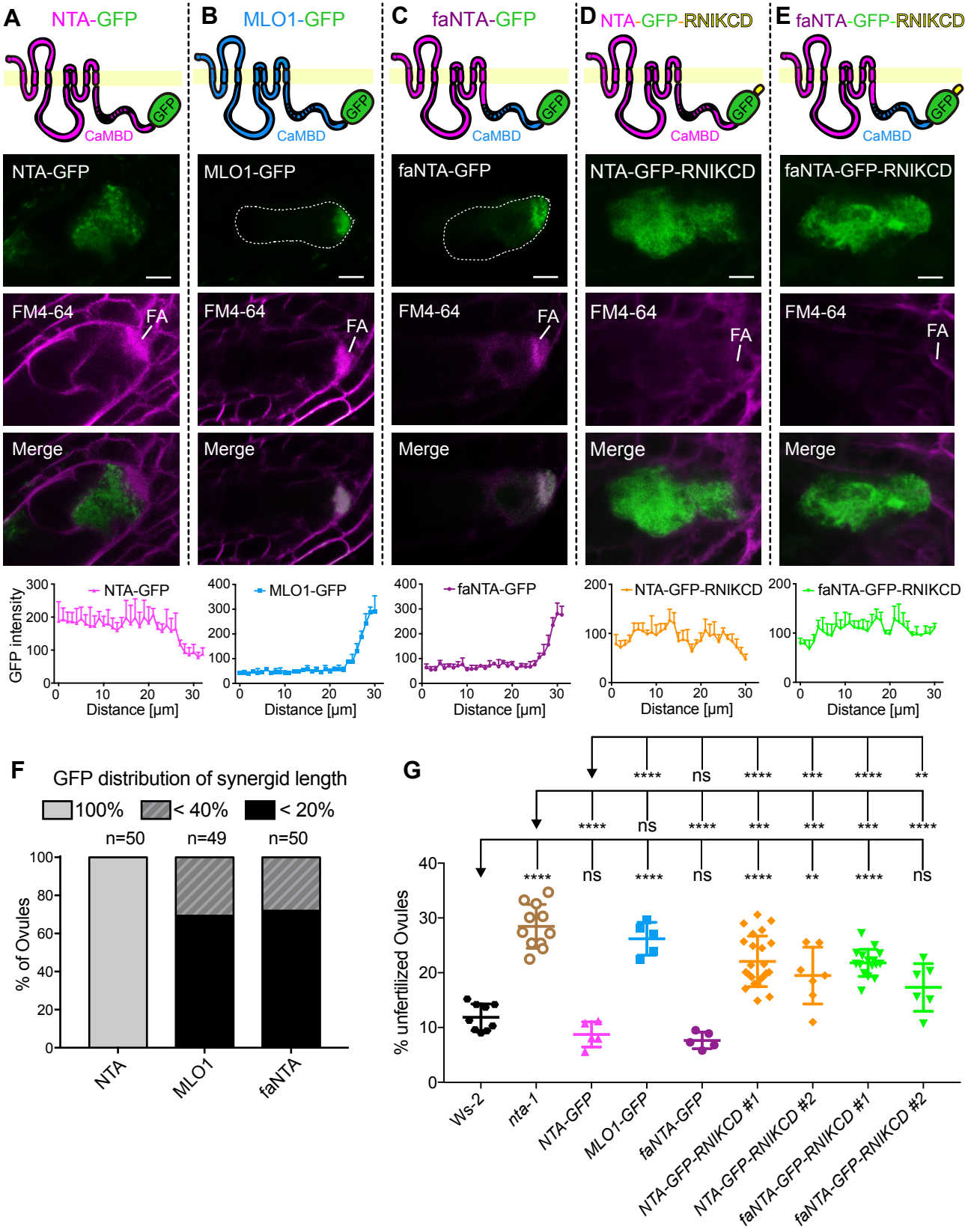
A
NTA-GFP
B
MLO1-GFP
C
faNTA-GFP
D
NTA-GFP-RNIKCD
E
faNTA-GFP-RNIKCD
GFP
CaMBD
FM4-64
FA
Merge
GFP intensity
Distance [µm]
F
GFP distribution of synergid length
100%
< 40%
< 20%
n=50
n=49
n=50
% of Ovules
NTA
MLO1
faNTA
G
% unfertilized Ovules
****
ns
***
**
Ws-2
nta-1
NTA-GFP
MLO1-GFP
faNTA-GFP
NTA-GFP-RNIKCD #1
NTA-GFP-RNIKCD #2
faNTA-GFP-RNIKCD #1
faNTA-GFP-RNIKCD #2

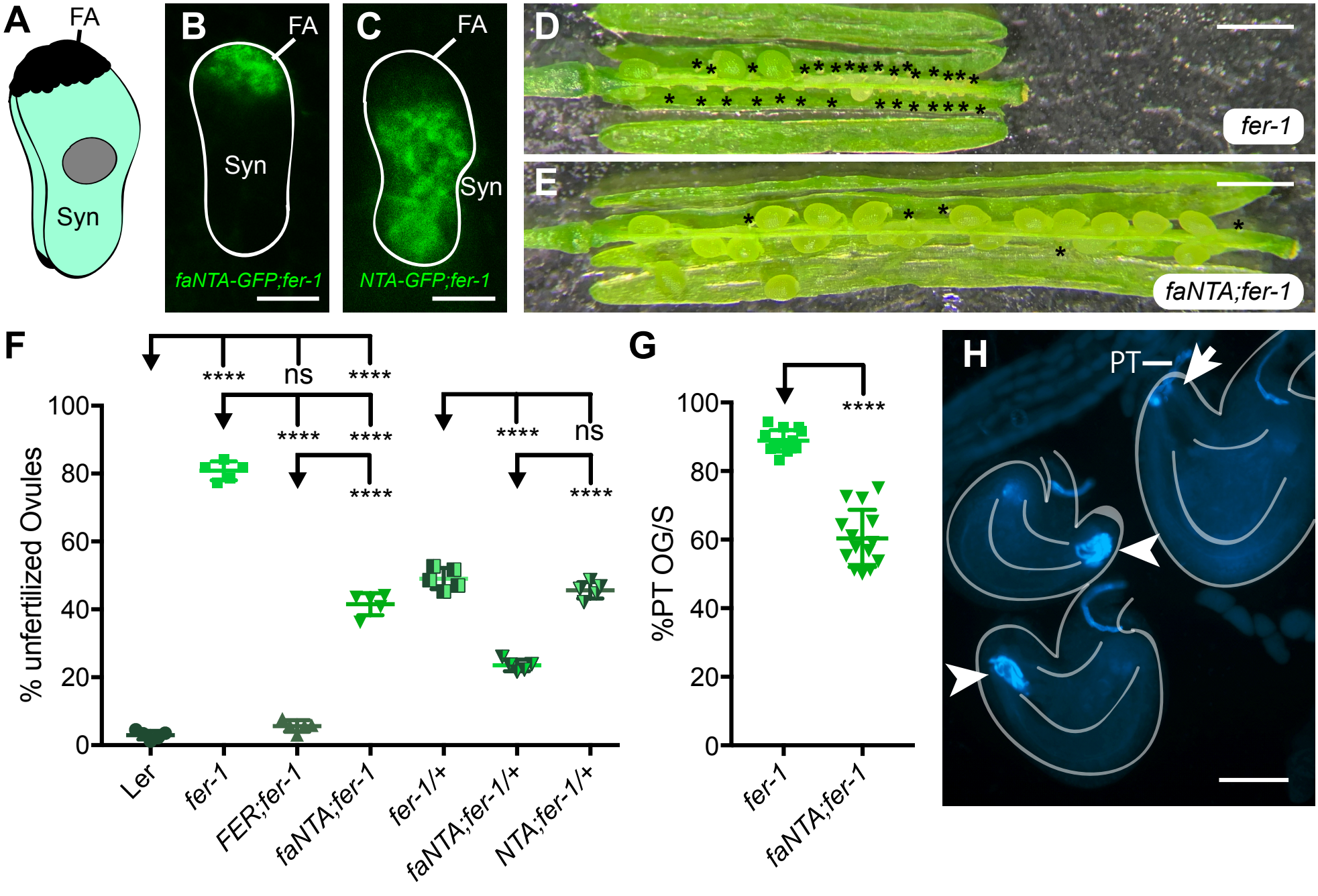
A
FA
Syn
B
FA
Syn
faNTA-GFP;fer-1
C
FA
Syn
NTA-GFP;fer-1
D
fer-1
E
faNTA;fer-1
F
% unfertilized Ovules
100
80
60
40
20
0
****
ns
****
****
****
****
****
ns
****
Ler
fer-1
FER;fer-1
faNTA;fer-1
fer-1/+
faNTA;fer-1/+
NTA;fer-1/+
G
%PT OG/S
100
80
60
40
20
0
****
fer-1
faNTA;fer-1
H
PT

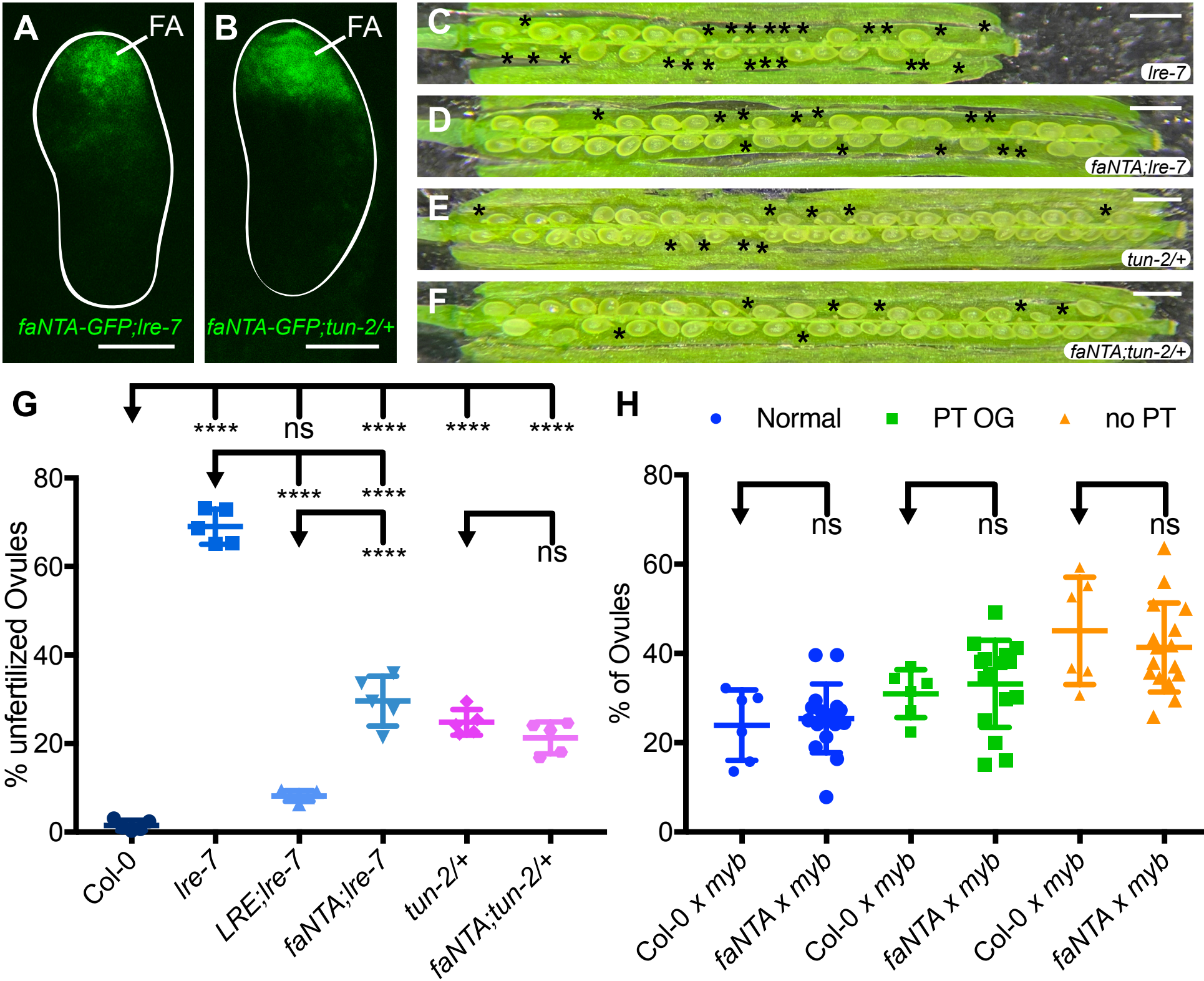
A
FA
faNTA-GFP;lre-7
B
FA
faNTA-GFP;tun-2/+
C
lre-7
D
faNTA;lre-7
E
tun-2/+
F
faNTA;tun-2/+
G
% unfertilized Ovules
0
20
40
60
80
****
ns
****
****
****
****
****
ns
Col-0
lre-7
LRE;lre-7
faNTA;lre-7
tun-2/+
faNTA;tun-2/+
H
Normal
PT OG
no PT
% of Ovules
0
20
40
60
80
ns
ns
ns
Col-0 x myb
faNTA x myb
Col-0 x myb
faNTA x myb
Col-0 x myb
faNTA x myb

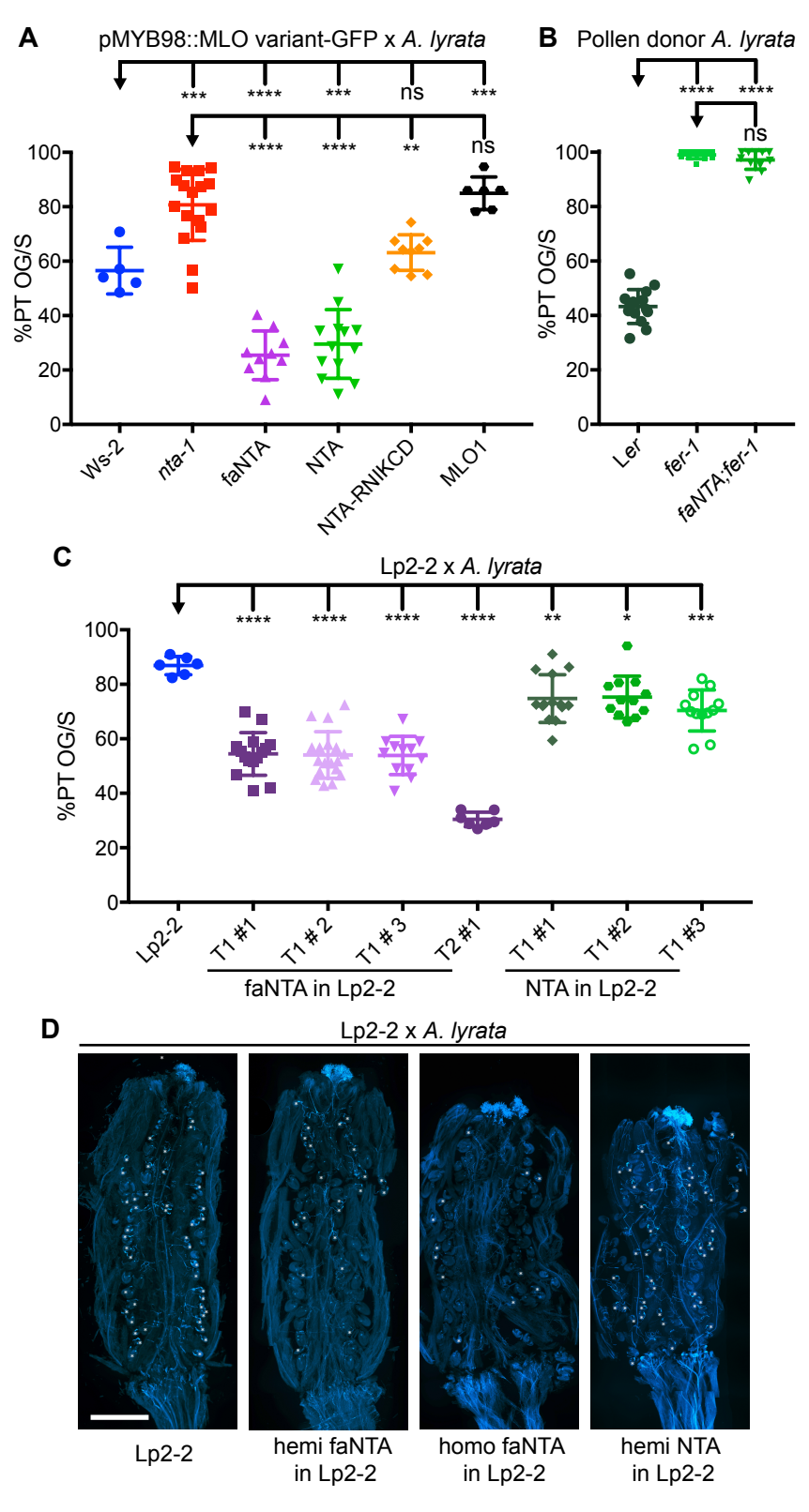
A
pMYB98::MLO variant-GFP x A. lyrata
%PT OG/S
Ws-2
nta-1
faNTA
NTA
NTA-RNIKCD
MLO1
B
Pollen donor A. lyrata
Ler
fer-1
faNTA;fer-1
C
Lp2-2 x A. lyrata
Lp2-2
T1 #1
T1 # 2
T1 # 3
T2 #1
T1 #1
T1 #2
T1 #3
faNTA in Lp2-2
NTA in Lp2-2
D
Lp2-2 x A. lyrata
Lp2-2
hemi faNTA in Lp2-2
homo faNTA in Lp2-2
hemi NTA in Lp2-2

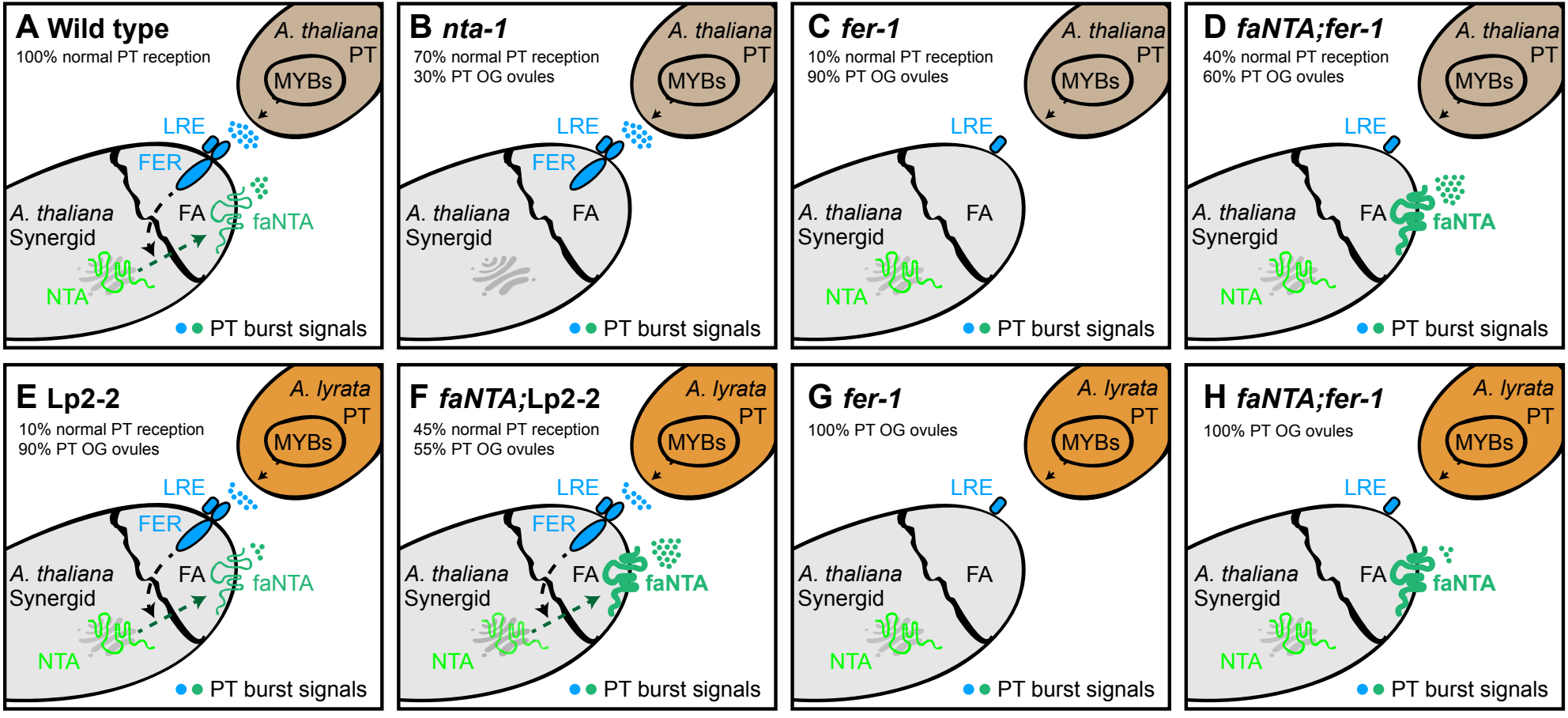
A Wild type
100% normal PT reception
A. thaliana PT
MYBs
LRE
FER
A. thaliana Synergid
FA
faNTA
NTA
PT burst signals
B nta-1
70% normal PT reception
30% PT OG ovules
C fer-1
10% normal PT reception
90% PT OG ovules
D faNTA;fer-1
40% normal PT reception
60% PT OG ovules
E Lp2-2
10% normal PT reception
90% PT OG ovules
A. lyrata PT
F faNTA;Lp2-2
45% normal PT reception
55% PT OG ovules
G fer-1
100% PT OG ovules
H faNTA;fer-1
100% PT OG ovules

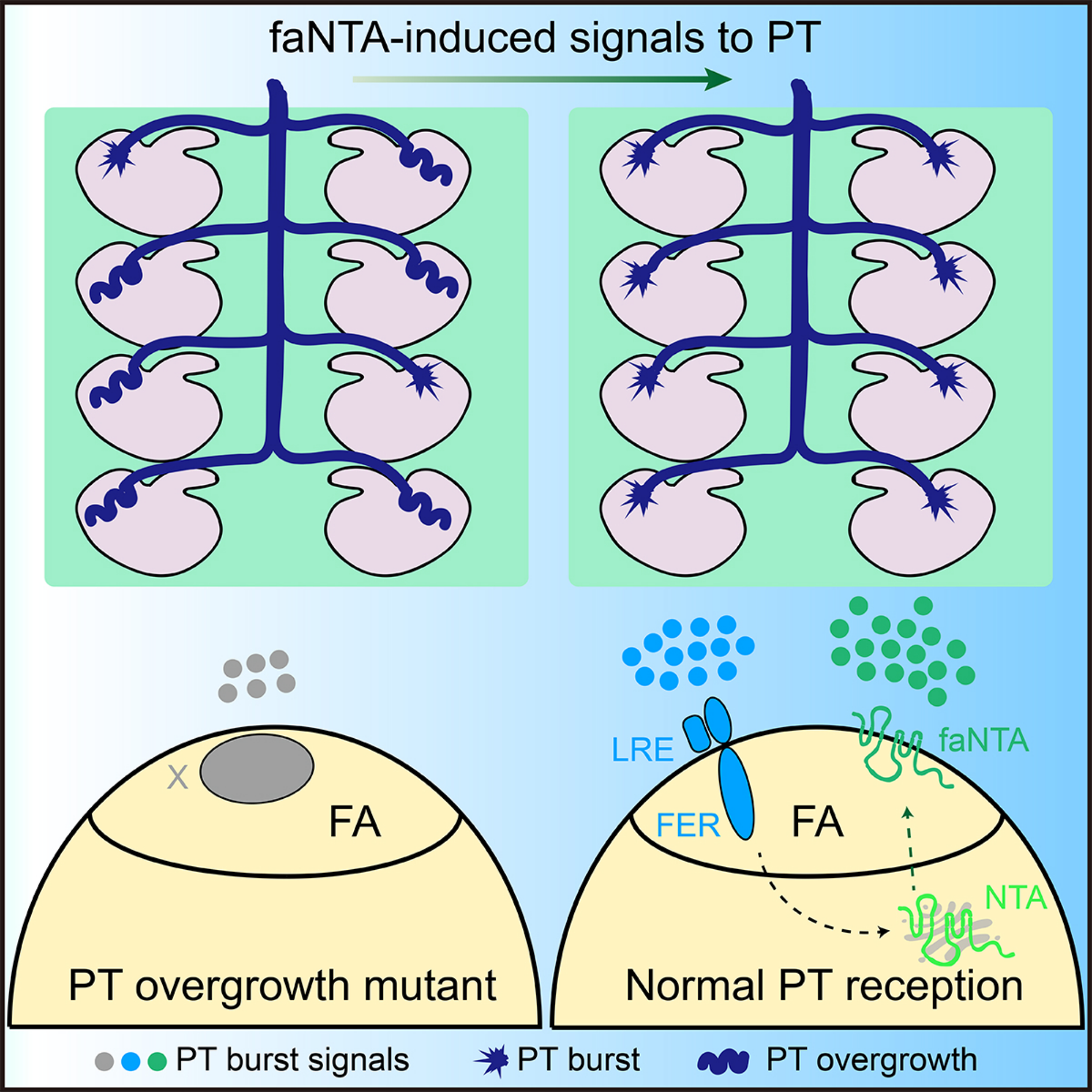
faNTA-induced signals to PT
X
FA
PT overgrowth mutant
LRE
FER
faNTA
FA
NTA
Normal PT reception
PT burst signals
PT burst
PT overgrowth